Pergamon

Geochimica et Cosmochimica Acta, Vol. 68, No. 3, pp. 557–571, 2004

0016-7037/04 $30.00 + .00

doi:10.1016/S0016-7037(03)00460-5

Precipitation kinetics and carbon isotope partitioning of inorganic siderite at 25°C and 1 atm

CONCEPCIÓN JIMENEZ-LOPEZ[1,†] and CHRISTOPHER S. ROMANEK[1,2,*]

[1]Savannah River Ecology Laboratory, Drawer E, Aiken SC, 29802 USA
[2]Department of Geology, University of Georgia, Athens, GA 30602 USA

(*Received May* 22, 2002; *accepted in revised form June* 24, 2003)

Abstract—Siderite was precipitated from $NaHCO_3$ and $Fe(ClO_4)_2$ solutions under anaerobic conditions at 25°C and 1 atm total pressure using a modified version of the chemo-stat technique and the free-drift technique. Samples of solution and solid were withdrawn at different time intervals during time course experiments to determine the bulk and isotope composition of the solution and solid, and the morphology and mineralogy of the solid. A series of metastable precursors precipitated and dissolved sequentially, culminating in well-crystallized siderite rhombohedra having an average edge of ~ 2 μm and a limited size distribution. Siderite precipitation rate ranged from $10^{0.23}$ to $10^{2.44}$ μmol•m^{-2}•h^{-1} for saturation states (with respect to siderite) ranging from near equilibrium to $10^{3.53}$. Calculated carbon isotope fractionation factors ($10^3 \ln\alpha$) averaged 8.5 ± 0.2 (1σ; n = 4) for the siderite-$CO_{2(g)}$ system and 0.5 ± 0.2 (1σ; n = 4) for the siderite-$HCO_3^-{}_{(aq)}$ system. *Copyright © 2004 Elsevier Ltd*

1. INTRODUCTION

Siderite ($FeCO_3$) is the most common authigenic carbonate in iron-bearing sediments of all ages (James, 1966; Perry and Tan, 1972; Hangari et al., 1980; Maynard, 1982; Thyne and Gwinn, 1994; Fisher et al., 1998). Siderite has been found on Earth in a broad range of environments including: lake sediments (Emerson, 1976; Bahrig, 1985; Kelts, 1988), estuaries (Bricker, 1985), carbonate-rich springs (Michard et al., 1988) and shallow to deeply buried sediments and rocks (Mozley, 1989; Rajan et al., 1996). Siderite has also been identified in extraterrestrial materials, such as meteorites (Romanek et al., 1994; Valley et al., 1997; Treiman and Romanek, 1998) and interplanetary dust particles (Keller et al., 1994). Siderite formation is known to be facilitated by both mesophilic and thermophilic iron reducing bacteria (Zhang et al., 1998, 2001; Romanek et al., 2003), and has been interpreted to be microbially mediated in many natural environments (Curtis et al., 1986; Moore et al., 1992; Mozley and Carothers, 1992; Coleman and Raiswell, 1993; Duan et al., 1996; Mortimer and Coleman, 1997).

Despite the wide occurrence of siderite, little is known about the chemical conditions in which inorganic siderite forms (i.e., precipitation kinetics or isotope partitioning between siderite and solution). This knowledge would facilitate a better understanding of the depositional and diagenetic processes that occurred in environments where siderite is found.

Most previous studies that synthesized siderite inorganically precipitated the solid from metastable precursors (phases that precipitated during the early stage of an experiment and dissolved thereafter, giving rise to more stable crystalline phases) under elevated temperatures or pressures (Carothers et al., 1988; Wersin et al., 1989; Bruno et al., 1992; Ptacek, 1992) or by recrystallizing precursors at temperatures ramping from 35°C to 70°C (Johnson, 1990). To our knowledge, Singer and Stumm (1970) were the only researchers who precipitated inorganic siderite at temperatures between 17°C and 30°C under atmospheric pressure and a relatively low P_{CO_2} environment (<10% CO_2). Siderite formed from solutions containing $NaHCO_3$, $HClO_4$ and $Fe(ClO_4)_2$ in free-drift experiments. These solutions were mixed and stored in bottles that were kept closed for several months in thermostatic baths at a specific temperature. However, their experimental procedures were described in brief terms, leaving much room for interpretation as to the exact protocols used and no information was provided on the evolution of solution chemistry over time.

Very little experimental data exist on carbon isotope partitioning between siderite and $CO_{2(g)}$. Golyshev et al. (1981) used a physical lattice model to calculate theoretical values for $10^3 \ln\alpha_{\text{sid-}CO_{2(g)}}$, where $\alpha_{\text{sid-}CO_{2(g)}}$ is the carbon isotope fractionation factor between siderite and $CO_{2(g)}$. They determined a value of 14.6 at 25°C. Carothers et al. (1988) determined $10^3 \ln\alpha_{\text{sid-}CO_{2(g)}}$ values for carbon at temperatures ranging from 33° to 197°C and pressures ranging from 100 to 500 bars. Extrapolation of their results to 25°C yields a value of 12.3, which is significantly lower than that predicted by Golyshev et al. (1981). Zhang at al. (2001) determined carbon isotope fractionation factors between biogenic siderite and $CO_{2(g)}$, using both mesophilic (15° to 35°C) and thermophilic (45° to 75°C) iron-reducing bacteria to facilitate the precipitation reaction. The results of Zhang et al. (2001) were consistent with Carothers et al. (1988) after a correction was made to the data of Carothers et al. (1988).

The goal of this study was to precipitate siderite inorganically at 25°C and 1 atm total pressure at relatively low P_{CO_2} under controlled physicochemical conditions. The precipitation kinetics and carbon isotope fractionation factors for the siderite-$CO_{2(g)}$ and siderite-$HCO_3^-{}_{(aq)}$ systems were determined

* Author to whom correspondence should be addressed (romanek@srel.edu).
† *Present address:* Microbiology Department, Facultad de Ciencias. Universidad de Granada, Campus de Fuentenueva, 18002 Granada, Spain

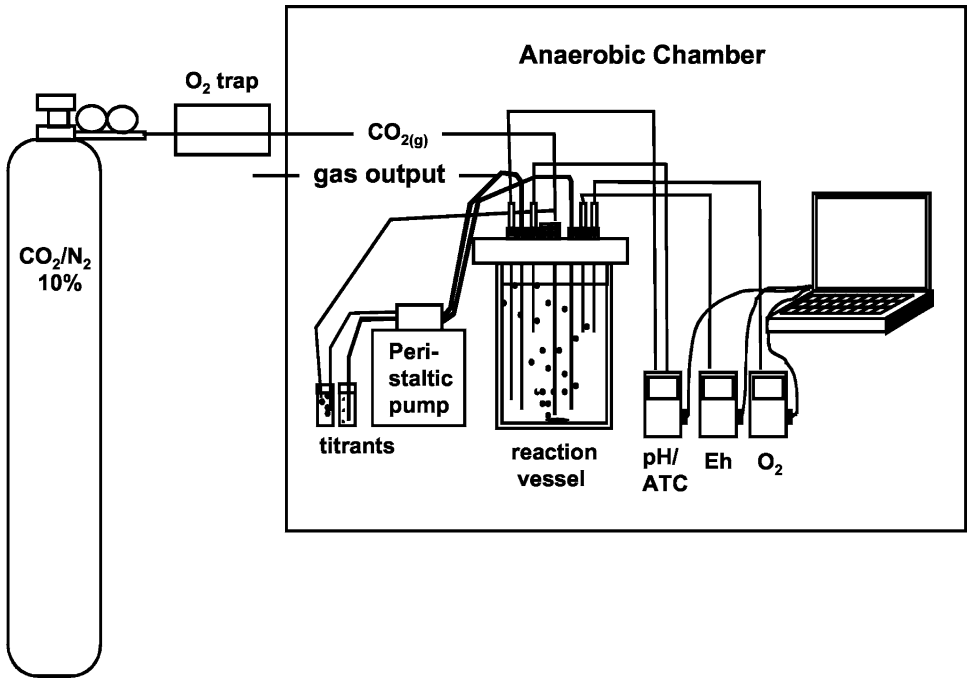

Fig. 1. Experimental chemo-stat system. Titrants ($NaHCO_3$ and $Fe(ClO_4)_2$ solutions) were fed into the master solution (shown here in the water-jacketed reaction vessel) to compensate for uptake of ions by the precipitation of a Fe-bearing carbonate, thereby maintaining a near constant pH and Eh. A CO_2/N_2 gas mixture, passed through an O_2 trap, was bubbled through the master solution and titrants to maintain chemical and carbon isotope equilibrium between solutions and carbon sources.

to more accurately and precisely constrain inorganic mechanisms for the origin of siderite.

2. MATERIAL AND METHODS

2.1. Materials

Sigma and Aldrich certified chemicals were used to prepare $NaHCO_3$ and $Fe(ClO_4)_2$ solutions in oxygen-free de-ionized water (Milli-Q). Oxygen free water was prepared by boiling 2L of de-ionized water for 1 h. This water was then cooled by sparging with ultrapure N_2 in a crushed ice bath. Once cold, the oxygen-free water was immediately placed inside an anaerobic chamber. Solutions of $NaHCO_3$ and $Fe(ClO_4)_2$ were prepared separately with oxygen-free water and bubbled for 4 and 2 h, respectively, with a certified 10% CO_2 gas mixture (N_2 balance), that was passed through a hot Cu furnace to remove trace O_2. Bubbling CO_2/N_2 through the solutions allowed for the saturation of these solutions with $CO_{2(g)}$, and for gaseous and aqueous carbon phases (DIC) to reach chemical and isotopic equilibrium at 25°C before the beginning of an experiment.

2.2. Methods

2.2.1. Experimental apparatus and analytical procedures

The experimental design used in this study is based on the chemo-stat technique where solution chemistry is regulated at steady state disequilibrium and seed material is introduced to constrain the mineralogical form of the solid precipitated (Morse, 1974). Isotope fractionation relations can be determined from these experiments, but they are very sensitive to the percentage of overgrowth when the mass of solid precipitated is small compared to the seed (Romanek et al., 1992). Because of the slow kinetics and sensitive nature of siderite precipitation to redox conditions, an alternative technique was devised in which a small mass of fine seed material was generated in the master solution through homogeneous nucleation before the regulation of solution chemistry. For the experiments reported here, the mineralogy of the initial precipitate was unclear, but the assumption was made that siderite overgrowth dominated the mass of solid precipitated even for samples collected relatively early in an experiment. Verification of this assumption was made by monitoring the mineralogy of the precipitate through the time course experiment. This technique permitted the determination of carbon isotope fractionation factors for siderite with considerably less error than the conventional seeded-growth technique.

Experiments were performed at 25°C and 1 atm total pressure inside an anaerobic chamber (COY Laboratory Products Inc.) filled with a H_2/N_2 (4% H_2) mixture (anaerobic grade). The chamber atmosphere was continually circulated through fans containing palladium catalyst to reduce trace O_2 to H_2O to maintain anaerobic conditions. The chamber also contained anhydrous $CaSO_4$ to trap any H_2O produced by the reaction of H_2 and O_2 on the palladium catalyst. The chamber was equipped with gas analyzers to continually monitor $O_{2(g)}$, $H_{2(g)}$ and $CO_{2(g)}$ levels throughout the course of an experiment.

Experiments were run in a water-jacketed reaction vessel having a lid (Fig. 1) that contained *o*-rings to ensure an air-tight seal. The lid contained *o*-ring compression ports for various probes, and input and output lines for titrants and gases. The master solution was stirred with a magnetic stirrer and bubbled using a disposable pipette. Titrants were transferred to the reaction vessel from reservoirs through tubing using a peristaltic pump. pH, Eh and $O_{2(aq)}$ were data-logged using probes and pH-meters interfaced to a computer-based data-logging system. The pH electrode was calibrated with standard buffer solutions for slope correction (pH 4 and 7). The Eh electrode was calibrated using quinhydrone in pH 4 (+273 mV) and 7 (+86 mV) buffers. The O_2 electrode was calibrated using oxygen-free water ($\sim$ +30 mV) and de-ionized water equilibrated with atmospheric O_2 ($\sim$ −600 mV). Based on the periodic measurement of calibrant standards, accuracy for pH was $\pm$ 0.05 (1σ), Eh was $\pm$3 mV (1σ) and O_2 was $\pm$ 10 mV (1σ).

Total iron concentration of the fluid was measured by inductively coupled plasma optical emission spectrometry (ICP-OES, Perkin-Elmer 4300DV.S) at a wavelength of 259.939 nm. One mL samples of solution were acidified with oxygen-free HCl (0.5 mol/L, 20 μL) to prevent the formation of solid before analysis. Analytical uncertainty

for ICP-OES was ± 0.03 mM (1σ). Analysis of total dissolved inorganic carbon (DIC: $H_2CO_{3(aq)} + CO_{2(aq)} + HCO_3^-{}_{(aq)} + CO_3^{2-}{}_{(aq)}$) was carried out by acidimetric titration of 10 mL of filtered solution (0.05 μm filter). The titration end point was calculated using the Gran function (Stumm and Morgan, 1981). Experimental error was ± 0.3 mM (1σ).

Solid mineralogy was determined using an X-ray diffractometer (Scintag, XGEN-4000). Powder samples were analyzed using CuKα radiation at an accelerating voltage of 35 kV and current of 40 mA. Each sample was covered with a wax membrane (parafilm) during analysis to minimize surface oxidation. The relative percentage of siderite in a mixed-mineralogy solid was calculated from the area of the (1 0 4) reflection peak for siderite, assuming a linear relationship between this peak area and the percentage of siderite in known standards analyzed at a mass equivalent to the samples.

The morphology of precipitate grains was determined using a field emission scanning electron microscope (LEO 982 FE-SEM). Samples were freeze dried and gold coated (150 Å in thickness) before SEM analysis.

All stable isotope measurements were made on a Finnigan Delta^{plus}XL isotope ratio mass spectrometer operated in continuous flow mode (CF-IRMS), using the Gasbench II peripheral device. The analytical methods included:

a) Solids: About 0.15–0.20 mg of solid was loaded in a 10 mL glass container having a removable top fitted with a septum (exetainer™, Labco). The exetainer was closed and flushed with He (UHP: ultra high purity grade) at 10 mL/min for 10 min. Next, 0.1 mL of 100% H_3PO_4 was injected in the exetainer (8 drops), making sure that acid completely covered the bottom of the container. The exetainer was then placed in a drying oven at 85°C over night.
b) DIC: Three drops of 100% H_3PO_4 was placed in an exetainer and the container was sealed and flushed as described above. One mL of sample solution was injected in the exetainer and the mixture was equilibrated at 25°C overnight.
c) $CO_{2(g)}$: An empty exetainer was closed and flushed as described above. Thirty five μL of 100% $CO_{2(g)}$ or 350 μL of a CO_2/N_2 gas mixture (10% $CO_{2(g)}$) was injected in the exetainer with a gas-tight syringe.

At least three samples of the international standard NBS-19 were run with each set of solid samples analyzed, and in-house standard solutions of $NaHCO_3$ (calibrated to V-PDB) were run with each set of liquid samples. Helium flushed and acid-loaded exetainers were run with each set of samples to correct for the background contribution (negligible) to measured carbon isotope values.

The method used to measure the stable isotope composition of $CO_{2(g)}$ in the headspace of an exetainer consisted of: 1) three measurements of reference gas $CO_{2(g)}$ injected in the He carrier gas of the CF-IRMS through an open split followed by, 2) ten consecutive measurements of exetainer headspace using a two-port syringe needle, capillary and a 100 μL sample loop, and 3) a final measurement of the reference gas. Flow conditions were 0.5 mL/min through the Gasbench II device and all the gases (UHP grade) used were passed through high purity gas scrubbers before introduction in the IRMS.

All isotope ratios determined from reference and sample injections were integrated and averaged, respectively, to improve the precision of the analysis. If individual area ratios for injections deviated by more than 10%, the data were discarded and the sample was analyzed again. Linearity checks were performed daily to ensure a response better than 0.05‰ per volt for $\delta^{13}C$ and $\delta^{18}O$ for $CO_{2(g)}$ before the measurement of samples. Based on the repeated analysis of standards and replicates, the analytical uncertainty was < 0.2 ‰ (1σ) for all measurements. All isotope measurements are reported in ‰ units versus the V-PDB standard using conventional delta (δ) notation (Craig, 1957).

2.2.2. Experimental procedure

Three different techniques were used to precipitate siderite in this study. In the first procedure, siderite was precipitated using the chemostat technique after allowing for the free drift nucleation of solid seed material (Fig. 1). These experiments are referred to as controlled-chemistry (CC) experiments; one experiment was run for 10 h (CC14), 12 h (CC-H), 230 h (CC18) and 240 h (CC20). At the conclusion of run CC20, a portion of the fluid and suspended solid were transferred to three 100 mL bottles, which were sealed with tightly fitting lids. These bottles constituted closed system reactors for a second set of experiments, the free-drift (FD20) experiments, which were terminated at 15, 45 and 60 d. Finally, a third set of experiments was conducted where solid was precipitated from master solutions stored in Pyrex bottles (1L) for one year. These experiments are referred to as long-term free-drift (FD-L) experiments (FD-L-3, FD-L-6, FD-L-9).

2.2.2.1. Controlled chemistry experiments (CC). To initiate a CC experiment, solutions of $NaHCO_3$ (0.875 L, 50 mM) and $Fe(ClO_4)_2$ (0.875 L, 34 mM), previously bubbled with a CO_2/N_2 gas mixture (10% CO_2), were mixed to form a master solution having a final concentration of 25mM $NaHCO_3$ and 17 mM $Fe(ClO_4)_2$. This master solution (1.75 L) was placed in the water-jacketed reaction vessel, the lid was securely fixed and the solution was stirred and bubbled at 300 mL min^{-1} with the 10% CO_2 gas mixture. Electrodes were introduced through ports and data-logged at one minute intervals for the duration of an experiment. Free-drift precipitation was permitted for 3 h for run CC14, and 72 h for runs CC18 and CC20. The solid that precipitated within this period acted as seed for the further heterogeneous growth of material. At this time, $NaHCO_3$ (0.5 mol/L) and $Fe(ClO_4)$ titrants (0.26 mol/L) were added that contained excess ion concentrations approximately identical in bulk and carbon isotope composition to those removed by the precipitation reaction. The rate at which the titrants were added was determined so as to hold the pH, alkalinity and $Fe^{2+}{}_{(aq)}$ concentration nearly constant over time. This technique worked well for pH and alkalinity but it was only marginally successful for $Fe^{2+}{}_{(aq)}$. Both titrants were bubbled with the same CO_2/N_2 gas mixture (10% CO_2) as the master solution for the entire experiment. See Table 1 for the time points at which samples were withdrawn.

To determine how the initial chemistry of the master solution affected the morphology and mineralogy of the initial precipitate, a related CC-H experiment was run at relatively high $NaHCO_3$ and $Fe(ClO_4)_2$ concentration [50 mM $NaHCO_3$/68 mM $Fe(ClO_4)_2$]. Titrants were introduced after 4 h and the experiment was terminated at 12 h (see Table 1).

Fifteen mL of solution and solid were withdrawn from the reaction vessel at each sampling event. The sample was filtered with a 0.05 μm Millipore membrane. Two mL was collected for stable isotope analysis, 10 mL was immediately analyzed for DIC, and 1 mL was acidified with 20 μL of oxygen-free HCl (0.5 mol/L) and diluted to 100 mL in oxygen-free de-ionized H_2O for total iron analysis. Sample containers were stored in a refrigerator, in the dark at 4°C for analysis. Solid was immediately recovered from the filter and freeze dried for morphological, mineralogical and stable isotope analysis. Solids were stored in the anaerobic chamber in vials and were not removed except for characterization.

2.2.2.2. Free-drift experiments (FD). At the conclusion of run CC-20 (240 h), three aliquots of master solution (containing $\sim$ 0.2 g solid each) were placed in 100 mL Pyrex bottles. The bottles were filled with solution, sealed with lids, and stored inside the anaerobic chamber for an additional 15, 45 and 60 d. At each one of these time intervals, a single bottle was opened and Eh, pH and O_2 were immediately measured. Solution and solid were prepared for mineralogical, chemical and isotope analysis as explained above.

2.2.2.3. Long term free-drift experiments (FD-L). Three stock solutions were prepared as in the CC experiments, the first (FD-L-3) with a final concentration of 10 mM $NaHCO_3$/50 mM $Fe(ClO_4)_2$ ($\Omega_{sid} = 10^{4.14}$), the second (FD-L-6) with a final concentration of 25 mM $NaHCO_3$/25 mM $Fe(ClO_4)_2$ ($\Omega_{sid} = 10^{3.56}$), and the third (FD-L-9) with a final concentration of 140 mM $NaHCO_3$ /5 mM $Fe(ClO_4)_2$ ($\Omega_{sid} = 10^{3.83}$). Solutions of $NaHCO_3$ and $Fe(ClO_4)_2$ were prepared separately with oxygen-free water and bubbled for 4 and 2 h, respectively, with pure CO_2 gas that was passed, before bubbling, through a hot Cu furnace to remove trace O_2. A different $CO_{2(g)}$ tank was used to bubble the master solution of each FD-L experiment. Each master solution was stored in a 1L Pyrex bottle that was filled, sealed with a lid, and kept in the anaerobic chamber for 1 yr. After this time, the bottles were opened,

Table 1. Measured values for pH, Eh, $Fe_{T(aq)}$, edge length (size) and alkalinity, calculated values for $HCO^{-}_{3\,(aq)}$, $CO^{2-}_{3\,(aq)}$, $CO_{2(aq)}$, mass of precipitate (solid), mass normalized surface area, saturation state with respect to siderite, and precipitation rate for four controlled chemistry (CC) experiments (CC14, CC18, CC20 and CC-H), three free drift (FD20) experiments (15, 45 and 60 days) and three long term free-drift (FD-L) experiments (FD-L-3, FD-L-6 and FD-L-9). Time step when titrants were injected is in bold italics. Time step when siderite was the primary solid is in bold underlined.

Run type	Time (hours)	pH	Eh (mV)	$Fe_{T(aq)}$ ($M\times10^{3}$)	Alkalinity ($M\times10^{3}$)	$HCO^{-}_{3\,(aq)}$ ($M\times10^{3}$)	$CO^{2-}_{3\,(aq)}$ ($M\times10^{6}$)	$CO_{2(aq)}$ ($M\times10^{5}$)	Solid (g)	Size (μm)	Surface area (m^2/g^{-1})	Log ($\Omega_{sid}-1$)	Log r (μmol $m^{-2}h^{-1}$)
CC14	0	7.15	−240	33.70	26.10	26.00	34	3.32	0	–	–	4.13	–
	2	7.30	−275	17.20	20.50	20.50	36	1.83		–	–	3.89	–
	3	7.30	−301	20.40	14.70	14.70	27	1.33	2.67	0.4	4.51	3.83	–
	4	7.23	−376	15.00	20.10	20.00	31	2.13	3.79	0.5	3.16	3.75	
	5	7.23	−388	9.97	28.90	28.80	46	3.05	4.81	0.6	2.63	3.72	
	10	7.28	−423	5.13	40.00	39.90	72	3.73	5.85	1.0	1.58	3.61	
CC18	0	6.72	−235	17.60	25.00	25.00	11	11.20	0	–	–	3.43	–
	5	7.41	−400	5.67	1.05	1.05	2	9.39	2.41	0.5	3.17	2.30	–
	20	7.23	−380	9.54	8.77	8.75	12	1.24	1.63	0.8	2.00	3.23	–
	25	7.12	−383	9.23	8.17	8.15	9	1.39	1.69	0.8	1.86	3.11	1.90
	30	7.16	−382	7.94	5.56	5.55	7	0.87	1.92	0.9	1.75	2.92	2.44
	35	7.16	−384	8.10	5.90	5.89	7	0.92	1.95	1.0	1.66	2.96	1.48
	45	7.16	−385	7.46	4.85	4.84	6	0.76	2.03	1.0	1.53	2.84	1.55
	50	7.16	−386	7.58	4.61	4.60	6	0.72	2.05	1.1	1.48	2.82	1.21
	72	7.16	−386	4.73	9.54	9.53	12	1.48	2.60	1.2	1.31	2.92	1.98
	90	7.16	−395	4.94	13.60	13.60	17	2.11	3.83	1.3	1.21	3.07	2.27
	110	7.16	−401	5.36	16.50	16.50	21	2.57	4.41	1.4	1.14	3.16	1.70
	130	7.16	−412	3.94	16.70	16.70	21	2.60	4.84	1.5	1.07	3.01	1.57
	150	7.16	−412	4.74	21.30	21.30	26	3.32	5.39	1.5	1.02	3.17	1.66
	170	7.16	−414	3.24	21.40	21.40	26	3.33	6.42	1.6	0.98	2.99	1.91
	190	7.16	−408	1.89	21.70	21.60	27	3.38	7.43	1.7	0.95	2.75	1.84
	230	7.16	−408	2.79	29.50	29.40	38	4.59	8.72	1.8	0.89	3.02	1.60
CC20	0	6.87	−255	16.2	25.00	25.00	16	7.58	0	–	–	3.57	–
	5	7.40	−385	4.64	1.86	18.60	4	0.17	2.53	0.5	3.17	2.47	–
	20	7.20	−370	7.98	8.50	8.49	12	1.21	1.66	0.8	2.00	3.15	–
	25	7.18	−369	8.18	8.92	8.91	11	1.32	1.62	0.8	1.86	3.16	–
	72	7.12	−397	7.08	14.20	14.20	15	2.43	1.82	1.2	1.31	3.23	–
	90	7.12	−391	9.71	22.20	22.20	25	3.79	1.84	1.3	1.21	3.53	0.64
	130	7.12	−392	7.30	23.40	23.40	26	4.00	3.46	1.5	1.07	3.39	2.29
	150	7.12	−398	7.29	26.50	26.40	31	4.51	4.04	1.5	1.02	3.43	1.51
	170	7.14	−407	5.40	25.70	25.60	31	4.18	5.01	1.6	0.98	3.29	1.84
	190	7.14	−406	6.81	31.50	31.40	38	5.13	5.29	1.7	0.95	3.46	1.18
	240	7.15	−410	3.17	31.80	31.70	39	5.06	7.53	1.8	0.88	3.11	1.63
CC-H	0	7.46	−346	67.70	49.90	49.650	160	3.85	0	–	–	4.91	–
	1	7.35	−415	61.40	37.10	36.90	91	4.99	1.28	2.0	0.79	4.64	–
	2	7.27	−417	55.00	24.90	24.80	51	6.07	2.47	3.0	0.53	4.35	–
	4	7.22	−418	59.10	32.20	32.10	58	6.78	1.73	3.0	0.53	4.44	–
	5	7.22	−420	61.70	36.70	36.60	68	6.78	1.25	3.0	0.53	4.51	–
	6	7.21	−422	51.50	17.40	17.30	30	2.43	3.36	4.0	0.39	4.11	–
	7	7.19	−424	61.50	36.60	36.50	63	5.36	1.40	5.0	0.32	4.47	–
	12	7.18	−430	56.90	27.10	27.00	45	4.02	2.61	5.0	0.32	4.39	–
FD20	15 days	7.24	−169	0.66	26.60	26.60	37	3.80	0.24	1.9	0.85	3.11–2.40	0.55
FD20	45 days	7.21	−289	2.01	25.50	25.40	19	3.62	0.25	2.0	0.79	3.11-equil	0.36
FD20	60 days	7.20	−199	0.15	25.50	25.40	19	3.62	0.25	1.9	0.83	3.11–1.74	0.23
FD-L-3	0	7.43	−520	50.00	10.00	9.96	22	0.72	0	–	–	4.14	–
	1 year	5.72	−227	32.60	4.55	4.54	0.2	22.40	2.26	7.5	0.21	1.91	–
FD-L-6	0	6.74	−349	25.10	25.00	25.00	11	9.09	0	–	–	3.56	–
	1 year	6.93	−162	11.10	9.85	9.84	11	2.79	1.95	3.8	0.42	2.98	–
FD-L-9	0	7.83	−368	5.00	139	140	64	0.43	0	–	–	3.83	–
	1 year	7.12	−270	0.23	102	102	120	14.60	6.47	5.6	0.28	2.49	–

Eh, pH and O_2 were measured, and solid and solution were collected and analyzed as explained above.

2.2.3. Calculations

2.2.3.1. Saturation state and precipitation rate. Saturation state with respect to siderite (Ω_{sid}) was calculated by dividing the ionic activity product of $a(Fe^{2+})\cdot a(CO_3^{2-})$ by the solubility product for siderite ($10^{-10.8}$; Bruno et al., 1992), where a = mγ, m = molality and γ = activity coefficient. Activity coefficients were calculated from the measured pH, cation concentration and alkalinity of the solution using a model developed by Romanek et al. (1992). This model was amended to include association constants for $(FeCl)^{+}_{(aq)}$, $FeOH^{+}_{(aq)}$, $(FeHCO_3)^{+}_{(aq)}$ (Nordstrom et al., 1990), $(FeCO_3)^{0}_{(aq)}$ and $Fe(CO_3)^{2-}_{2(aq)}$ (Bruno et al., 1992). See Table 2 for details. Because the reagent $Fe(ClO_4)_2$ was used under anaerobic conditions, $Fe_{T(aq)}$ was

Table 2. Relevant ion pair constants at 25°C and 1 atm.

Log K	Value	Reference
$FeCO_3 \leftrightarrow Fe^{2+} + CO_3^{2-}$	−10.8	Bruno et al. (1992)
$Fe^{2+} + Cl^- \leftrightarrow (FeCl)^+$	0.14	Nordstrom et al. (1990)
$Fe^{2+} + H_2O \leftrightarrow H^+ + FeOH^+_{(aq)}$	−9.5	Nordstrom et al. (1990)
$Fe^{2+} + HCO_3^- \leftrightarrow (FeHCO_3)^+_{(aq)}$	2.0	Nordstrom et al. (1990)
$Fe^{2+} + CO_3^{2-} \leftrightarrow (FeCO_3)^0_{(aq)}$	5.5	Bruno et al. (1992)
$Fe^{2+} + 2CO_3^{2-} \leftrightarrow Fe(CO_3)^{2-}_{2\,(aq)}$	7.1	Bruno et al. (1992)

assumed to be Fe^{2+}. Perchlorate ion was considered as chloride ion in the calculations as Hood et al. (1954) concluded that perchloric acid is highly dissociated even in highly concentrated solutions.

Precipitation rate, r, was calculated for all time intervals (except run CC-H) where siderite was identified as the predominant phase (>50%) in the solid as determined by XRD analysis (Table 3). Precipitation rate was calculated from the following parameters: 1) the amount of $Fe^{2+}_{(aq)}$ added from the titrants and the change in $Fe^{2+}_{(aq)}$ concentration of the master solution over a particular time interval (to calculate the mass of $FeCO_3$ that precipitated), 2) the surface area of preexisting crystals that acted as seed for the heterogeneous growth of solid over a time interval, and 3) the length of a time interval. Mass normalized estimates of surface area (m^2g^{-1}) were determined from the average edge length of rhombohedra recovered during sampling intervals and a geometrical model (for details, see Jiménez-López et al., 2001). The total surface area available for the heterogeneous growth of a solid over a particular time interval was determined from the product of the seed mass and normalized surface area from the preceding time interval. Siderite precipitation rate was determined by dividing the mass of $FeCO_3$ produced (as $Fe^{2+}_{(aq)}$ consumed) over an interval by the total surface area from the previous time step. Precipitation rate was calculated in this manner for runs CC18, CC20 and the FD20 experiments because the mass of seed material that acted as substrate was known for particular time intervals and the precipitate was greater than 50% siderite. Because seed material was not introduced in the FD-L experiments, precipitation rate could not be constrained for this set of runs. Finally, precipitation rates for run CC-H could not be determined because of erratic fluctuations in the mass of solid available for the heterogeneous growth of siderite over some time intervals. This was probably a result of the relatively high saturation state of this experiment (with respect to siderite), and the precipitation and dissolution of significant mass(es) of metastable phases during this experiment (see below).

2.2.3.2. Carbon isotope fractionation factors ($10^3 ln\alpha$). The difference in isotope composition between two components of a system is described by the isotope fractionation factor (α), where

$$\alpha_{A-B} = R_A/R_B = (\delta_A + 1000)/(\delta_B + 1000) \quad (1)$$

for components A and B, with $R_X = {}^{13}C/{}^{12}C$ for compound (X = A or B) and

$$\delta_x = 1000\left[\frac{R_x - R_{st}}{R_{st}}\right] \quad (2)$$

where st is a standard material.

The carbon isotope composition of individual components of the carbonic acid system ($CO_{2(aq)}$, $HCO_3^-{}_{(aq)}$, and $CO_3^{2-}{}_{(aq)}$) was computed from the $\delta^{13}C$ of DIC ($\delta^{13}C_{DIC}$), and measured values of pH, alkalinity and solution chemistry (e.g., $Fe^{2+}_{(aq)}$) using the ion speciation model and carbon isotope fractionation factors ($10^3 ln\alpha$) for the $HCO_3^-{}_{(aq)}$-$CO_{2(g)}$-$CO_3^{2-}{}_{(aq)}$ (Halas et al., 1997), $HCO_3^-{}_{(aq)}$-$CO_{2(g)}$ (Szaran, 1997), and $CO_{2(g)}$-$CO_{2(aq)}$ (Vogel et al., 1970) systems. Perchlorate ion ($ClO_4^-{}_{(aq)}$) was treated as Cl^- (as described above) and $Na^+_{(aq)}$ concentration was calculated from the stochiometry of the reagents used to make the stock solutions and titrants. The isotope composition of aqueous bicarbonate ion, $\delta^{13}C_{HCO3^-(aq)}$, was calculated from the following mass balance:

$$\delta^{13}C_{HCO_{3(aq)}^-} = \delta^{13}C_{DIC} - X_{CO_{2(aq)}}\,1000\ln\alpha_{CO_{2(aq)}-HCO_{3(aq)}^-} - X_{CO_{3(aq)}^{2-}}\,1000\ln\alpha_{CO_{3(aq)}^{2-}-HCO_{3(aq)}^-} \quad (3)$$

To determine when the DIC of the master solution reached carbon isotope equilibrium with the $CO_{2(g)}$ component of a $CO_{2(g)}/N_{2(g)}$ gas mixture, a theoretical value for $\delta^{13}C_{DIC}$ was calculated from the measured $\delta^{13}C$ value of tank gas CO_2, pH, and solution chemistry at 25°C.

The carbon isotope fractionation factor between siderite and $CO_{2(g)}$, $10^3 ln\alpha_{sid\text{-}CO_{2(g)}}$, was determined from Eqn. 1 and measured values for $\delta^{13}C_{solid}$ and $\delta^{13}C_{CO_{2(g)}}$ (or calculated $\delta^{13}C_{CO_{2(g)}}$ value for FD-L experiments, see Table 3) over time interval(s) for which the solid was composed of at least 95% siderite (except FD20 experiments, see below). This criteria is more restrictive than for the characterization of precipitation rate, where time intervals containing at least 50% siderite were considered in the calculation. This was done because the calculation of $10^3 ln\alpha$ is relatively sensitive to distinct isotope partitioning among metastable phase(s) relative to the calculation of precipitation rate (Jiménez-López et al., 2001). The carbon isotope fractionation factor between the siderite and $HCO_3^-{}_{(aq)}$, $10^3 ln\alpha_{sid\text{-}HCO_3^-{}_{(aq)}}$, was determined similarly using Eqn. 1, and the complementary measured value for $\delta^{13}C_{solid}$ and the calculated value for $\delta^{13}C_{HCO_3^-{}_{(aq)}}$ (see Eqn. 3).

3. RESULTS AND DISCUSSION

3.1. Chemical Composition

The experimental measurements of $O_{2(aq)}$, Eh and pH of the master solution are shown in Figure 2a over time for a representative CC experiment (CC20). At the beginning of an experiment, $O_{2(aq)}$ of the master solution was ~ +50 mV compared to the de-oxygenated water standard value of ~ +30 mV. Between 3 and 10 d, $O_{2(aq)}$ concentration stabilized at a value close to 0 mV. Before the initiation of a run, the Eh of the master solution was between −255 and −235 mV (e.g., Fig. 2a; Table 1). During a run, Eh decreased within 5 to 10 h to a minimum value, followed by a short-lived increase before it decreased again to less than −400 mV.

Eh is a function of the activity ratio of Fe^{3+}/Fe^{2+} in solution (i.e., Eh will increase when the concentration of $Fe^{2+}_{(aq)}$ decreases or Fe^{3+} increases). In the CC experiments, ferric ion ($Fe^{3+}_{(aq)}$) could be present in the master solution at very low concentration due to impurities in the reagents or as a result of the inadvertent oxidation of Fe^{2+} during the preparation of the stock or master solutions. The initial sharp drop in Eh may be related to the formation of a phase that mainly contained Fe^{3+}; it is well known that Fe^{3+}-bearing solids are highly insoluble compared to Fe^{2+}-phases at the pH of these runs (Stumm and Morgan, 1981). However, given the fact that such extreme measures were taken to exclude O_2 from the experiments, and that new certified reagents were used to prepare solutions, the drop in Eh could also be due to variations in $Fe^{2+}_{(aq)}$ over time. The concentration of $Fe^{2+}_{(aq)}$ is sensitive to ion pair formation and the precipitation and dissolution of metastable Fe^{2+}-bearing phases during the precipitation of a solid. The ephemeral increase in Eh after 10 h and subsequent decrease thereafter are probably due to small changes in $Fe^{2+}_{(aq)}$ (or Fe^{3+}) that occurred as titrants were injected in the master solution, or the precipitation and dissolution of various Fe-bearing solids during a run. Total $Fe_{(aq)}$ measurements and XRD/SEM analyses support this contention.

The pH of the initial master solution ranged from 6.7 to 7.2 for the CC experiments (except run CC-H). It increased to

Table 3. Percentage of siderite and carbon isotope data for the CC experiments (CC14, CC18, CC20 and CC-H), the free drift (FD20) experiments (15, 45 and 60 days) and long-term free drift (FD-L) experiments (FD-L-3, FD-L-6 and FD-L-9). No isotope data are available for run CC18 at 230 hours because the tank gas was switched during the run. Time step when titrants were injected is in bold italics. Time step when siderite was the greater than 50% of the solid is in bold underlined. Values used for determination of average $10^3\ln\alpha$ values are underlined.

Run type	Time (hours)	Siderite (%)	$\delta^{13}C_{DIC}$ (‰)	$\delta^{13}C_{solid}$ (‰)	$\delta^{13}C_{HCO_3^-}$ (‰)	$10^3\ln\alpha_{solid\text{-}DIC}$	$10^3\ln\alpha_{solid\text{-}HCO_3^-}$	$10^3\ln\alpha_{solid\text{-}CO_{2(g)}}$
CC14 (−43.5‰)[1]	0	no solid	−5.8	no solid	−4.7	no solid	no solid	no solid
	2	0	−31.6	−30.24	−30.8	1.4	0.6	13.8
	3	0	−33.8	−32.83	−33.0	1.1	0.2	11.1
	4	45	−34.1	−32.10	−33.2	2.0	1.1	11.9
	5	42	−34.4	−33.50	−33.5	1.0	0.0	10.4
	10	59	−35.3	−36.82	−34.4	−1.6	−2.5	7.0
CC18 (−21.6‰)[1]	5	45	−12.3	trace	−11.7	–	–	–
		–	–	–	–	–	–	–
	20	79	−12.3	−13.3	−11.4	−1.0	−2.0	8.4
		–		−13.4	–	−1.1	−2.0	8.4
	25	67	−11.2	−13.9	−10.1	−2.8	−3.9	7.8
		–	–	−13.8	–	−2.7	−3.7	7.9
	30	75	−14.5	−13.5	−13.5	1.0	0.0	8.3
		–	–	−13.7	–	0.7	−0.3	8.0
		–	–	−13.6	–	0.8	−0.2	8.1
	72	92	−14.4	−14.0	−13.4	0.4	−0.6	7.7
	110	65	−14.3	−13.6	−13.4	0.7	−0.3	8.1
		–	–	−13.9	–	0.5	−0.5	7.8
		–	–	−13.8	–	0.5	−0.5	7.9
	150	86	−14.4	−13.9	−13.5	0.5	−0.5	7.8
	170	80	−14.9	−14.0	−14.0	1.0	0.0	7.8
	190	83	−15.0	−13.8	−14.0	1.2	0.2	7.9
CC20 (−22.1‰)[1]	0	–	−14.1	no solid	−12.3	no solid	no solid	no solid
	5	41	−14.2	trace	−12.6	–	–	–
	–	–	–	–	–	–	–	–
	72	90	−15.4	−13.4	−14.3	2.0	0.9	8.9
	–	–	–	−13.6	–	1.8	0.7	8.6
	–	–	–	−13.8	–	1.6	0.5	8.4
	90	92	−14.9	−13.1	−13.8	1.8	0.7	9.1
	130	83	−15.0	−12.5	−14.0	2.6	1.5	9.7
	–	–	–	−12.6	–	2.5	1.4	9.7
	150	91	−15.2	−13.4	−14.2	1.8	0.8	8.8
	–	–	–	−14.1	–	1.1	0.1	8.1
	–	–	–	−13.9	–	1.3	0.2	8.3
	170	85	−15.2	−12.7	−14.2	2.5	1.5	9.5
	190	90	−15.1	−13.2	−14.1	1.9	0.9	9.0
	–	–	–	−13.3	–	1.8	0.8	8.9
	–	–	–	−12.8	–	2.3	1.3	9.4
	240	96	−15.1	−13.7	−14.1	1.4	0.4	8.5
	–	–	–	−13.6	–	1.5	0.5	8.6
	–	–	–	−13.6	–	1.5	0.5	8.6
CC-H (−43.5‰)[1]	0	no solid	−4.9	no solid	−4.4	no solid	no solid	no solid
	1	15	−14.2	−15.76	−13.2	−1.6	−2.6	28.6
	2	53	−21.8	−20.06	−21.2	1.8	1.2	24.3
	4	57	−29.3	−25.77	−28.6	3.6	2.9	18.4
	5	72	−33.5	−30.36	−32.8	3.2	2.5	13.7
	6	70	−34.3	−33.51	−33.6	0.9	0.1	10.4
	7	65	−35.0	−33.27	−34.1	1.8	0.9	10.7
	12	63	−35.3	−33.12	−34.4	2.2	1.3	10.8
	–	–	–	−33.89	–	1.4	0.5	10.0
	–	–	–	−33.29	–	2.1	1.2	10.7
	–	–	–	−33.80	–	1.5	0.6	10.1
FD20 (−22.1‰)[1]	15 days	100	−15.2	−13.8	−14.3	–	–	
	45 days	100	−15.0	−14.0	−14.1	–	–	–
	60 days	100	−15.3	−14.2	−14.4	–	–	–
FD-L-3 (−47.7‰)[2]	1 year	100	−41.1	−39.9	−40.1	7.6	0.2	8.2
FD-L-6 (−36.3‰)[2]	1 year	100	−29.9	−28.0	−28.6	1.9	0.6	8.6
FD-L-9 (−8.1‰)[2]	1 year	100	−1.0	0.6	−0.1	1.6	0.7	8.7

[1] Measured $\delta^{13}C$ value for CO_2/N_2 gas mixture bubbled through master solution.

[2] Calculated $\delta^{13}C$ value for tank gas CO_2 bubbled through master solution. Value was determined from $\delta^{13}C_{DIC}$, pH and solution chemistry using model described in text.

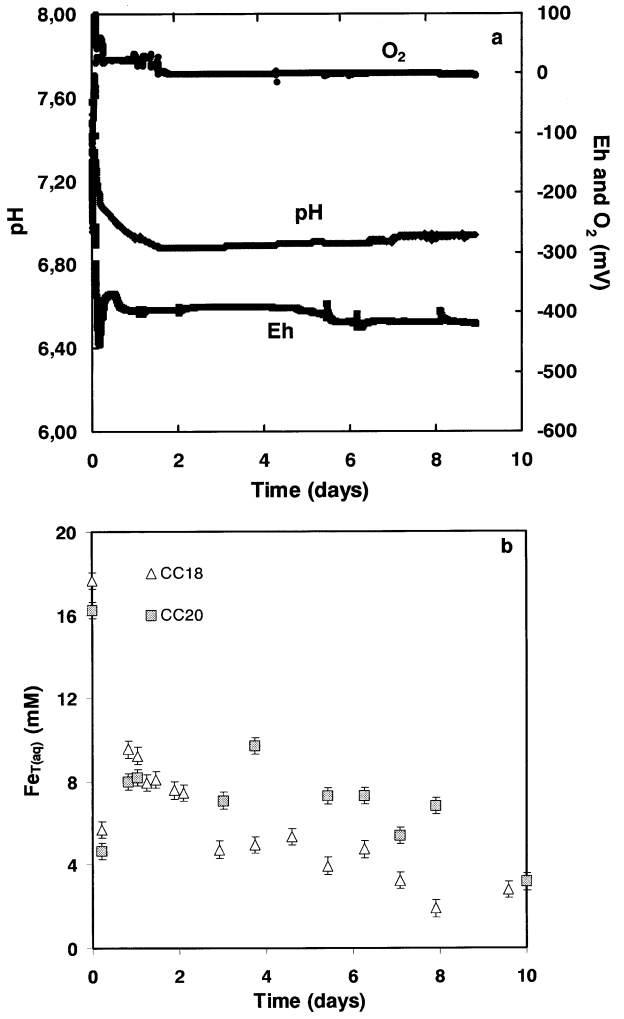

Fig. 2. Evolution over time of **a)** $O_{2(aq)}$, pH and Eh in the master solution of run CC20. Data were taken every minute for 10 d. Transient peaks in the profiles are associated with sampling events during the run, **b)** $Fe_{T(aq)}$ for two CC experiments (CC18 and CC20).

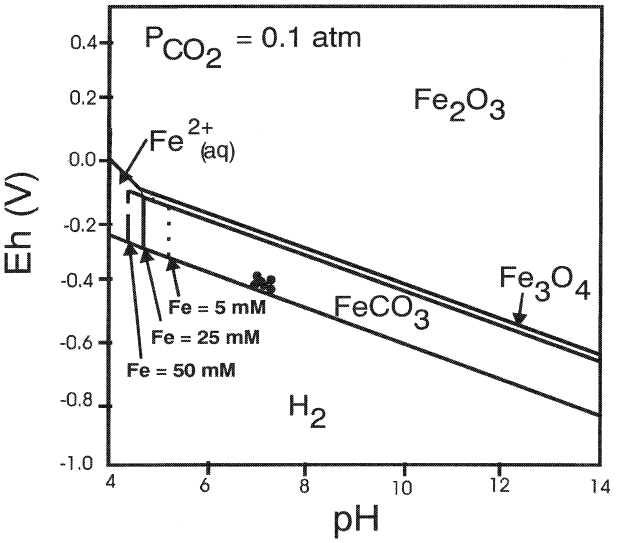

Fig. 3. Eh-pH diagram for the experimental conditions of all experiments (as black circles; P_{CO2} fixed at 0.1 atm).

about 7.4 by 5 h and then decreased to ~7.2 thereafter. The decrease occurred primarily within the time interval from 5 to 20 h. When the titrants were introduced, the pH of the solution stabilized and varied less than 0.07 pH units for the remainder of an experiment (e.g., Fig. 2a; Table 1).

Solution pH varied through time for several reasons including $CO_{2(aq)}$ degassing and acid generation during the homogeneous nucleation of carbonate during the early hours of an experiment. Degassing of $CO_{2(aq)}$ was an important process very early in the CC experiments because the calculated partial pressure of $CO_{2(g)}$ (P_{CO_2}) in equilibrium with the starting master solution was higher (0.2 atm.) than the P_{CO_2} of the stock solutions from which it was made (0.1 atm). As a consequence, $CO_{2(aq)}$ probably exsolved early on, raising the pH of the solution slightly until equilibrium with the gas phase was re-established. On the other hand, the resultant precipitation of solid carbonate will drive pH in the opposite direction as H^+ is liberated during the precipitation reaction. The subsequent decrease in solution pH can be explained by the precipitation of solid carbonate, which is consistent with the time when solid was first detected in the master solution.

The total iron in solution decreased to about 70% of the initial concentration within the first 5 h of a CC experiment (Table 1; excluding run CC-H). Total Fe increased by a factor of two shortly thereafter for the longer runs (CC18 and CC20), followed by a less severe but erratic decrease there after (Fig. 2b). The early decrease in $Fe_{T(aq)}$ was probably caused by the homogeneous nucleation of a Fe-bearing solid, while fluctuations there after may be attributed to the precipitation and dissolution of metastable phases (see below). These changes could not have resulted from the input of titrants as related fluctuations in pH also would have been observed.

An Eh-pH diagram was constructed for the experimental conditions of the experiments (Fig. 3: Garrels and Christ, 1990; Faure, 1991) to determine if the runs fall within the stability field of siderite or other Fe-bearing phases (e.g., Fe_3O_4, Fe_2O_3). The physicochemical conditions plot in the field where siderite is the thermodynamically favored phase. The concentration of $Fe^{2+}_{(aq)}$ has a strong role in determining the boundaries of the stability field for siderite: as the concentration of Fe^{2+} in solution is increased, the stability field for siderite increases, such that $FeCO_3$ is thermodynamically stable even at relatively low pH. This observation has important implications for the interpretation of carbon isotope fractionation relations presented below.

3.2. Morphology and Mineralogy of the Precipitate

Solid precipitate was first detected at between 1 and 3 h in the CC experiments. Two highly-reactive solids were observed consistently in the earliest run products. The first, and more reactive, crystalline phase had a habit (as seen in SEM photomicrographs) that was flattened and elongate in two directions and irregular in the third direction; it also displayed numerous kinks and steps on grain surfaces (Fig. 4a). This solid is

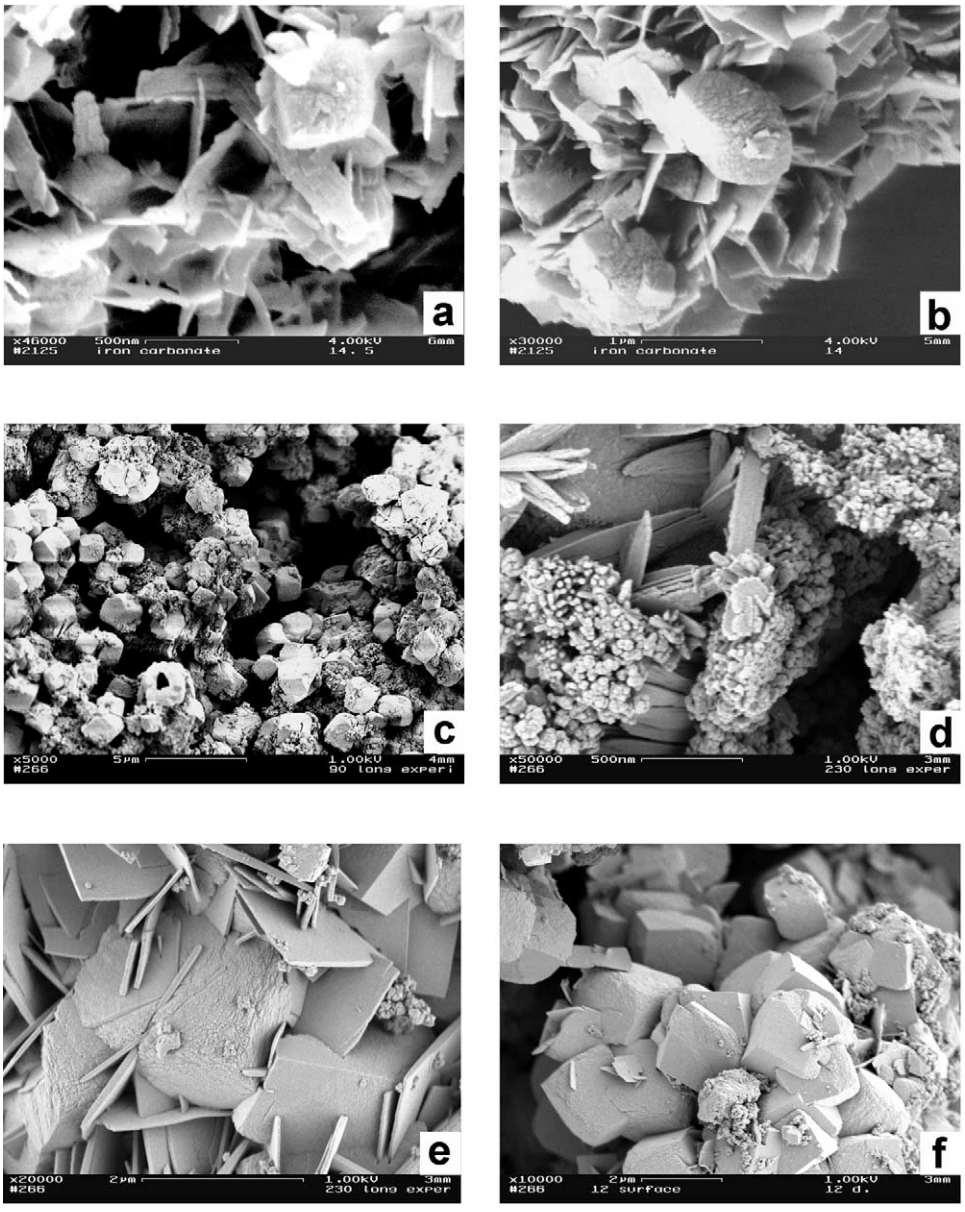

Fig. 4. SEM photo-micrographs of the solid during run CC18 at **a)** 5 h, **b)** 12 h, **c)** 3 d, **d, e)** 8 d, and **f)** 10 d; for free-drift experiment FD20 at **g)** 30 d, **h, i)** 45 d, and **j)** 60 d; and for long-term free-drift experiment FD-L-3, **k, l)** for 1 yr. The chemistry of the master solution at the beginning of the FD-L experiment was the same as in run CC18.

referred to as phase A because a mineralogical identification could not be made by XRD (see below). A few rhombohedral-shaped grains were detected at this time step. At about 12 h, phase A was still observed but a significant component of the solid was also rhombohedral in form (Fig. 4b). In addition, a third phase was first observed, referred to as phase B (again, crystalline but unidentifiable by XRD). This phase displayed an equant platy habit, with relatively well defined edges and vertices, and it lacked the numerous surface features characteristic of phase A (Fig. 4b). By 72 h, rhombohedra were commonly observed in SEM photo-micrographs (Fig. 4c–e), although phases A and B were still observed along with a very fine-grained form about 50 nm in diameter, which could be the nuclei of an existing or new phase. By 240 h, the solid was composed almost entirely of rhombohedra with a small percentage of phase B plates (Fig. 4f). Phase A was no longer detected in the solid at this point. At longer time intervals, neither phase A nor B were detected by SEM; rather the solid was composed of rhombohedra with rough crystal faces, displaying a high density of steps and kinks (Figs. 4g–j). SEM photo-micrographs of precipitate from the FD-L experiments, which were run for a year (e.g., FD-L-3: Figs. 4k, l), showed well-defined rhombohedra of about 8 μm in length, with faces that lacked the steps and kinks of earlier rhombohedra.

When sufficient material was available for XRD analysis ($\sim$ 15 mg), diffraction patterns displayed reflections characteristic of crystalline material (Fig. 5). XRD analyses of the solid from time steps up to 5 h displayed reflection peaks corresponding to

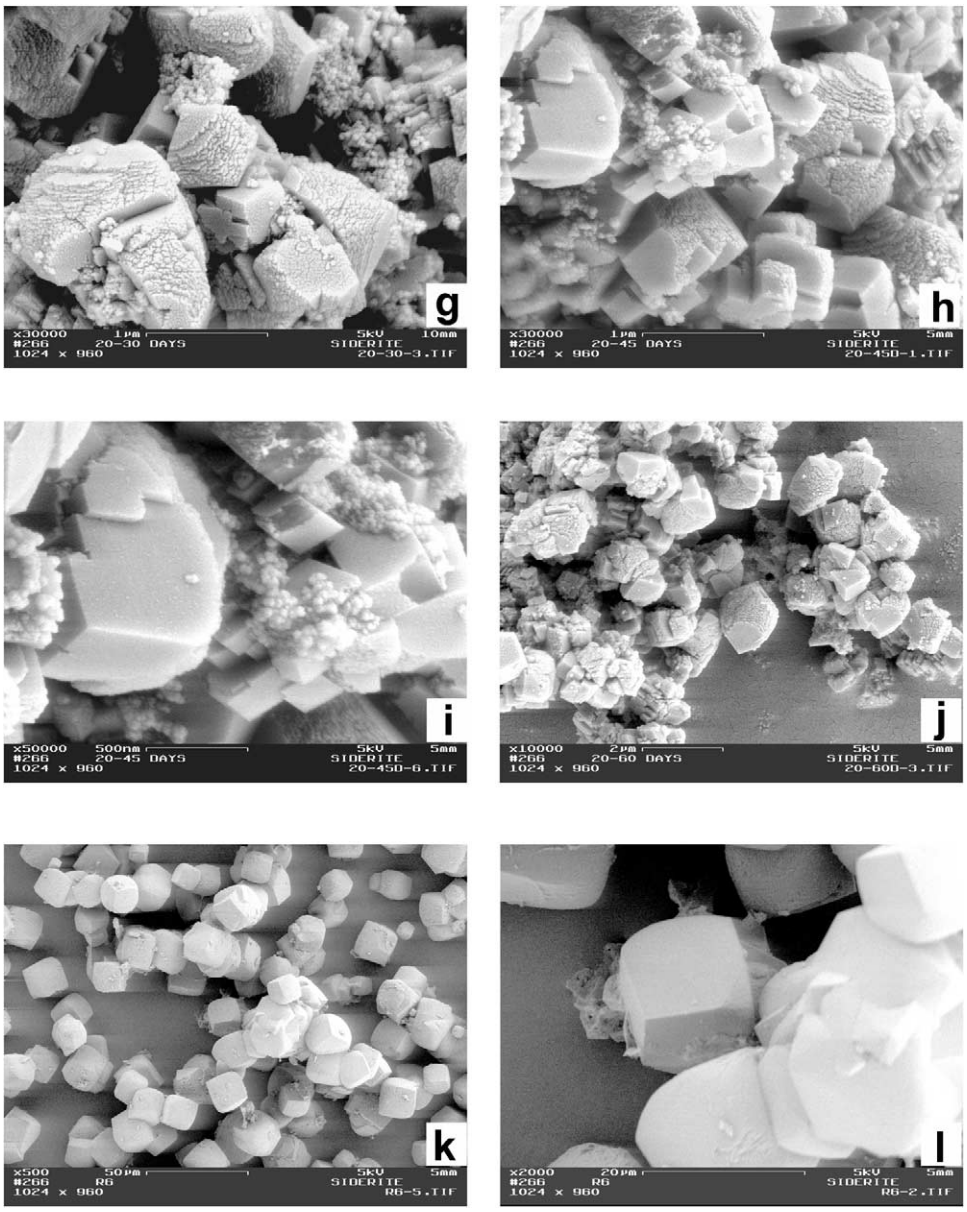

Fig. 4. (Continued)

siderite, and four other reproducible reflections at ~21.08°, 33.32°, 34.35° and ~36.37° (2θ; Fig. 5). These reflections (except for 34.35°) are probably associated with phase A, which was predominant at this time based on SEM analyses. At 12 h, reflections corresponding to siderite and phase A were detected along with a set of new, very reproducible reflections at ~28.80° and ~46.28° (2θ). These two reflections, along with 34.35°, probably correspond to phase B which was first noted in SEM photo-micrographs at this time interval.

The intensity of the reflections associated with siderite increased with time throughout the CC experiments. For instance, the intensity of the (1 0 4) reflection of siderite was about 6 times higher than any reflection of phase A and B after 5 h. Although this does not necessarily mean that siderite was the most prominent phase, it is likely, based on SEM analyses. Reflections corresponding to phase A were detected intermittently through 190 h (8 d), but they disappeared entirely by 240 h (10 d). Reflections corresponding to phase B were detected over the duration of an experiment, although more consistently toward the end of a run (240 h). Based on the XRD and SEM analysis, phase A is probably the irregular crystals that were detected early in the experiment and phase B is the more well-defined platey crystals that were observed later. The XRD analysis of the solid in both the FD and FD-L experiments only showed reflections for siderite. This result is consistent with the characteristic rhombohedral shape of grains observed by SEM for these runs. Based on XRD analysis, siderite was the predominant mineral phase in run CC14 at 10 h, while for runs CC18, CC20, and CC-H siderite was the predominant solid at 20, 72 and 2 h, respectively (see Table 3).

According to these results, the precipitation of iron carbonate minerals probably followed a sequential precipitation pathway.

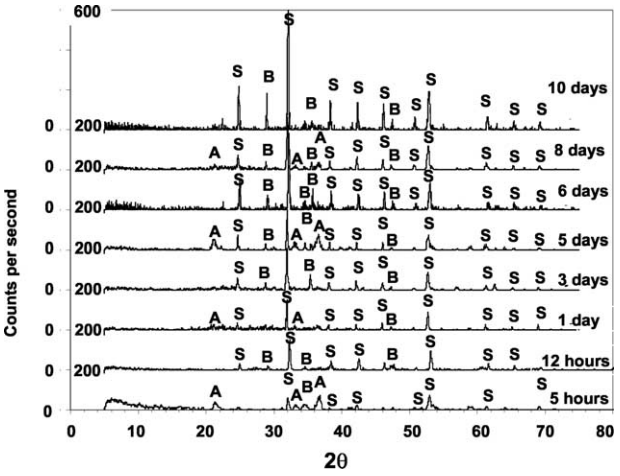

Fig. 5. X-Ray diffraction patterns of the solid collected during run CC18 from 5 h to 10 d. S = siderite, A = metastable phase A, B = metastable phase B. The intensity of the (104) peak for siderite exceeded 200 cps in most of the panels shown to facilitate comparison of minor peaks.

Phase A nucleated first at the highest saturation state with respect to siderite. The precipitation of this phase was kinetically favored compared to siderite, but over time it decreased in abundance (as observed by XRD and SEM) at the expense of phase B and siderite. This transformation probably proceeded as a dissolution-recrystallization sequence, which is consistent with changes in $Fe_{T(aq)}$ that were observed in the master solution over the early portion of a CC experiment (Fig. 2b). A similar behavior was previously observed in the precipitation of $CaCO_3$ from solution, where the most stable phase (calcite) precipitated after a chain of precipitation events in which less stable phases preferentially nucleated early and dissolved over time (Ogino et al., 1987; Jiménez-López et al., 2001). This mineral transition is consistent with the Ostwald Step Rule (Morse and Casey, 1988).

The higher initial saturation state of run CC-H compared to the other CC experiments did not promote the precipitation of a solid metastable with respect to phase A, although spherules were observed at 4 h (Fig. 6a). The spherulitic form was probably an amorphous phase which is commonly observed in highly supersaturated environments (Sears, 1961; García-Ruiz and Amorós, 1980). Phase A and B solids, and siderite rhombohedra were observed over the time course (Figs. 6b and 6c), but siderite rarely exceeded ~ 50% of the solid.

3.3. Precipitation Rate and Saturation State

Based on the predominance of siderite in the solid, precipitation rate was calculated for run CC18 over the time interval from 20 to 230 h, and run CC20 over the time interval from 72 to 240 h (see Tables 1 and 3). Siderite precipitation rate ranged from $10^{0.64}$ to $10^{2.44}$ μmol·m^{-2}·h^{-1} for log(Ω − 1) values that

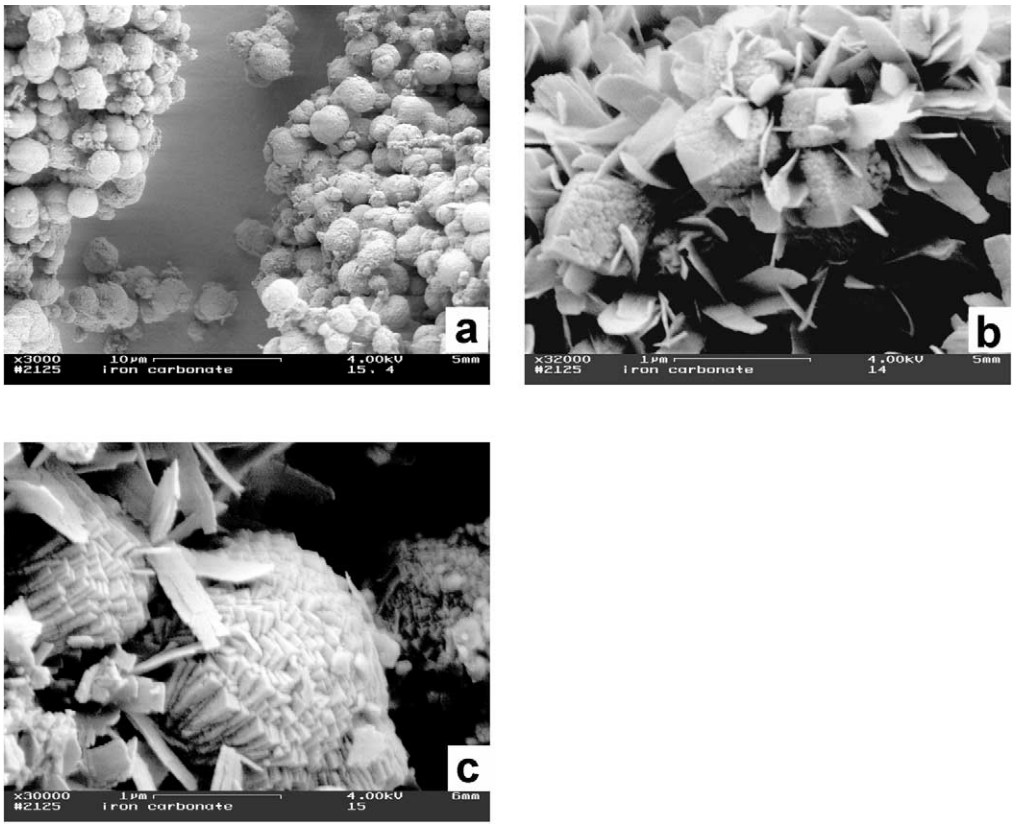

Fig. 6. SEM photo-micrographs of precipitate from run CC-H. Master solution: $NaHCO_3$ 50 mM/$Fe(ClO_4)_2$ 68 mM at **a)** 4 h and **b, c)** 12 h.

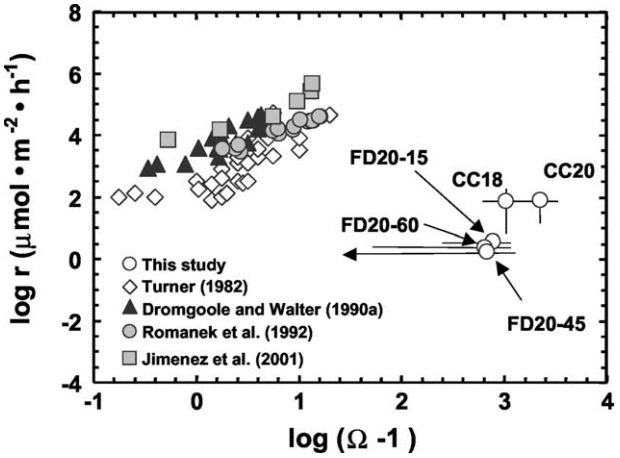

Fig. 7. Precipitation rate for siderite as a function of saturation state for runs CC18, CC20, and the free-drift (FD20) experiments (15 d, 45 d and 60 d). Error bars through symbols are minimum and maximum values of a run. Error bar with arrow represents near equilibrium conditions. Data are compared to calcite by Turner (1982); recalculated by Romanek et al. (1992), Dromgoole and Walter (1990a), Romanek et al. (1992), and Jiménez-López et al. (2001).

ranged from $10^{2.75}$ to $10^{3.53}$. Precipitation rates for the FD20 experiments ranged from $10^{0.23}$ to $10^{0.55}$ μmol·m^{-2}·h^{-1} for saturation states ranging from near equilibrium to $10^{3.11}$. Time-weighted average precipitation rates and saturation states for these runs are plotted in Figure 7. Bars through each average define the minimum and maximum values obtained for an experimental run. Parameters such as reaction order and rate constant are often determined from a linear regression of log-transformed data (Nancollas and Reddy, 1971; Reddy and Nancollas, 1971; Morse, 1978; Morse and Berner, 1979; Mucci and Morse, 1983). Although the data from this study can be modeled using a linear least squares fit, there is much uncertainty in the relationship because of variability in precipitation rate for the CC experiments and saturation state for the FD experiments. Nevertheless, the data may be compared to published values for calcite to gain a sense of the relative reaction kinetics of these two minerals under similar environmental conditions (Fig. 7). Based on this comparison, the saturation state of a solution must be approximately 3 orders of magnitude higher with respect to siderite compared to calcite for these two minerals to grow at comparable precipitation rates. Put another way, if the relationship between precipitation rate and saturation state is extrapolated for calcite to include the range of saturation states investigated for siderite in this study, then siderite precipitation rate is $\sim$ 8 orders of magnitude lower than calcite at comparable saturation states. The presence of Fe^{2+} has been shown to significantly lower the kinetics of calcite nucleation and precipitation at concentrations as low as 20 μM (Meyer, 1984; Dromgoole and Walter, 1990a, 1990b). Also, it has been observed previously from carbonate minerals (e.g., Mg-calcites) that precipitation rate is inversely related to the average surface density charge of the cation (Lippmann, 1973; Reddy and Wang, 1980; Mucci and Morse, 1983, Mucci, 1987; Deleuze and Brantley, 1997, Jiménez-López et al., in press). This is important because the energy required to dehydrate cations on the crystal surface increases with surface density

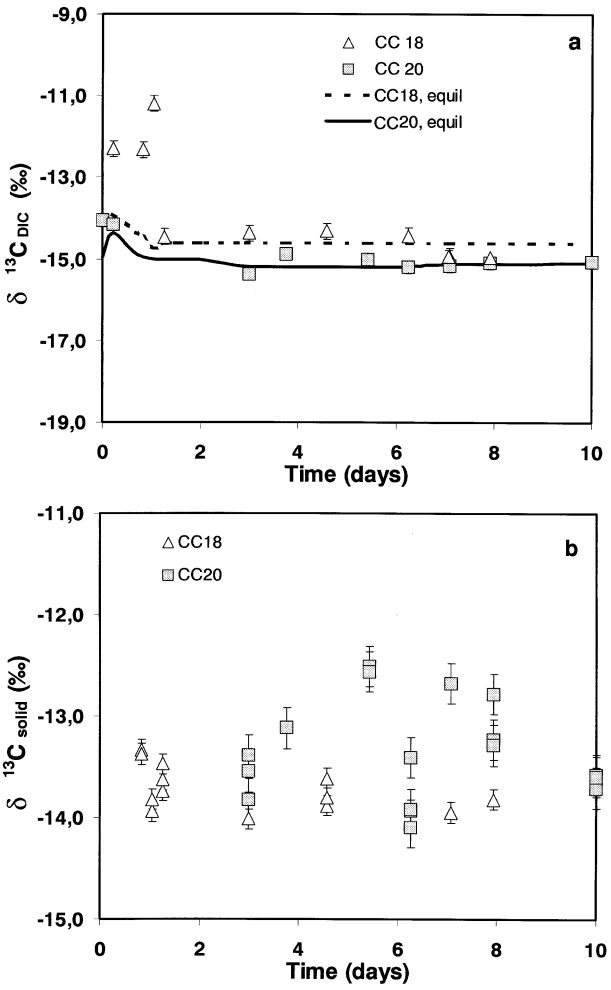

Fig. 8. Evolution of **a)** $\delta^{13}C_{DIC}$ and **b)** $\delta^{13}C_{solid}$ during runs CC18 and CC20.

charge (Lippmann, 1973). Because the ionic radius of Fe^{2+} and Fe^{3+} are smaller than Ca^{2+} (0.74 Å, 0.64 Å and 0.99 Å, respectively; Klein and Hurlbut, 1985), the surface density charge of Fe^{2+} is higher than Ca^{2+} and therefore, so is the energy required to dehydrate Fe^{2+} on the crystal surface. This may account for the greater activation energy required to form siderite (ranging from 51 $\pm$ 14 kJ/mol to 129 $\pm$ 50 kJ/mol; Johnson, 1990) compared to calcite (38.3 kJ/mol: Nancollas and Reddy, 1971; 39.2 kJ/mol: Kazmierczak et al., 1982).

3.4. Carbon Isotope Fractionation

Carbon isotope data are reported for all the experiments of this study in Table 3. Measured and theoretical $\delta^{13}C_{DIC}$ values are plotted for two CC experiments, runs CC18 and CC20, to monitor the evolution of $\delta^{13}C_{DIC}$ values over time and demonstrate the carbon isotope relationships between gaseous and aqueous carbon species during representative time course experiments (Fig. 8). The isotope composition of total dissolved inorganic carbon ($\delta^{13}C_{DIC}$) ranged from -15.0 ‰ to -11.2 ‰ in run CC18, and from -15.4 ‰ to -14.1 ‰ in run CC20,

with a general decrease in $\delta^{13}C$ over time (Table 3; CO_2/N_2 gas mixture in run CC18 was changed before 230 h so isotope data for this time interval are not reported). Equilibrium $\delta^{13}C_{DIC}$ values were calculated using the $\delta^{13}C$ value of $CO_{2(g)}$ in the gas mixture bubbled through the master solution and the physicochemical conditions of a run. For the first 90 h (<4 d) of run CC18, $\delta^{13}C_{DIC}$ values were up to 2 ‰ higher than the predicted value for isotope equilibrium with $CO_{2(g)}$. For run CC20, $\delta^{13}C_{DIC}$ values were also higher until 72 h (3 d), at which time they approximated the equilibrium curve. Departures from equilibrium in these early stages of the CC experiments may be explained by the exsolution of $CO_{2(aq)}$ from solution. This exsolution caused the pH to increase in the early hours of the experiments (see Fig. 2a) and may have induced the preferential exsolution of $CO_{2(aq)}$ relatively enriched in ^{12}C (Usdowski et al., 1979; Michaelis et al., 1985; Usdowski and Hoefs, 1990). For this reason, no carbon isotope data from time intervals earlier than 90 h were considered for the calculation of fractionation factors.

The $\delta^{13}C$ of the solid ($\delta^{13}C_{solid}$) was similar in runs CC18 and CC20 and ranged from ~ -14.1 ‰ to ~ -12.5 ‰ (Table 3, Fig. 8b). The variability in $\delta^{13}C_{solid}$ values within and between experiments was probably related to temporal changes in $\delta^{13}C_{DIC}$ and the precipitation and dissolution of metastable phases. These phases may have influenced the isotope systematics of early time points differentially if isotope fractionation among phases were distinct, and/or the percentage of phases changed through time. As stated earlier, the characterization of fractionation relations for carbonate minerals is sensitive to the presence of multiple phases in the precipitate, especially when these phases have distinct isotope compositions [for details on these effects, see McCrea (1950), Emrich et al. (1970), Turner (1982), Romanek et al. (1992), and Jimenez et al. (2001)].

To avoid potential problems associated with isotope disequilibrium between DIC and $CO_{2(g)}$, values, and multi-mineralic mixtures for the CC experiments, only run CC20 at 240 h (96% siderite) was used to characterize carbon isotope fractionation relations for siderite. The fractionation factor for the siderite-$CO_{2(g)}$ system ($10^3\ln\alpha_{sid\text{-}CO_{2(g)}}$) for this time interval was 8.6 ± 0.1 (n = 3; determined from $\delta^{13}C_{CO_2}$ and three replicate analyses of the solid, see underlined data in Table 3). The corresponding value for $10^3\ln\alpha_{sid\text{-}HCO_3^-(aq)}$ was 0.5 ± 0.1 (n = 3), using the $\delta^{13}C$ value for HCO_3^- calculated from the measured $\delta^{13}C_{DIC}$ value and the physicochemical conditions of this time interval.

The $\delta^{13}C$ of total dissolved inorganic carbon (DIC) in the FD20 experiments ranged from −15.3 ‰ to −15.0 ‰ and the $\delta^{13}C$ of the solid ($\delta^{13}C_{solid}$) ranged from −14.2 ‰ to −13.8 ‰ (Table 3). Both $\delta^{13}C_{DIC}$ and $\delta^{13}C_{solid}$ values were very close to those of run CC20 at 240 h. The amount of overgrowth obtained in the FD20 experiments was small (40 mg) though compared to the mass of the seed (0.2 g) so the isotope composition of the solid strongly reflected the $\delta^{13}C$ value of the seed. Because of this reason, the FD20 experiments were not considered in further calculations of $10^3\ln\alpha$ despite the fact they contained pure siderite.

Values for the isotope composition of DIC in the FD-L experiments were −41.1 ‰, −29.9 ‰ and −1.0 ‰ (Table 3). These differences are related to the different $\delta^{13}C$ values for $CO_{2(g)}$ that was bubbled through each master solution before the initiation of an experimental run. The corresponding $\delta^{13}C$ values for the solid (100% siderite) were −39.9‰, −28.0‰ and 0.6‰ (Table 3). Calculated fractionation factors ($10^3\ln\alpha_{sid\text{-}CO_{2(g)}}$) for these runs were 8.2 (FD-L-3), 8.6 (FD-L-6) and 8.7 (FD-L-9), while $10^3\ln\alpha_{sid\text{-}HCO_3^-(aq)}$ values were 0.2 (FD-L-3), 0.6 (FD-L-6) and 0.7 (FD-L-9). These values are in good agreement given the wide range of $\delta^{13}C$ values for $CO_{2(g)}$ that were used in these experiments. Combining the data for run CC20 at 240 h and the three FD-L experiments yields an average $10^3\ln\alpha_{sid\text{-}CO_{2(g)}}$ value of 8.5 ± 0.2 (n=4) and an average $10^3\ln\alpha_{sid\text{-}HCO_3^-(aq)}$ value of 0.5 ± 0.2 (n=4).

Values of $10^3\ln\alpha_{sid\text{-}CO_{2(g)}}$ and $10^3\ln\alpha_{sid\text{-}HCO_3^-(aq)}$ reported in this study are compared to theoretical values obtained by Golyshev et al. (1981), and experimental values determined by Carothers et al. (1988) and Zhang et al. (2001) in Figures 9a, b and Table 4. Golyshev et al. (1981) calculated the carbon isotope fractionation factor for the siderite and $CO_{2(g)}$ system using a physical lattice model. The extrapolation of their values for $10^3\ln\alpha_{sid\text{-}CO_{2(g)}}$ to 25°C yields a value of 14.6 ‰, which is greater than the value determine in this study (8.6 ± 0.2 ‰). Carothers et al. (1988) reported $10^3\ln\alpha_{sid\text{-}CO_{2(g)}}$ values ranging from 4.5 at 197°C to 11.6 at 33°C (Fig. 9a). The extrapolation of Carothers' data to 25°C yields a value of 12.3, again which is greater than that obtained in the present study. Carothers et al. (1988) measured $\delta^{13}C_{sid}$ and $\delta^{13}C_{DIC}$ in their experiments and calculated the $\delta^{13}C$ for $CO_{2(g)}$ from $\delta^{13}C_{DIC}$, assuming the $\delta^{13}C$ of DIC and HCO_3^- were equivalent. They used the $10^3\ln\alpha_{HCO_3^-(aq)}$-$CO_{2(g)}$ value at 20°C given by Friedman and O'Neil (1977) to relate the $\delta^{13}C$ value of $HCO_3^-{}_{(aq)}$ to $CO_{2(g)}$. There are two considerations in these calculations that affect the outcome of their results. As discussed in Zhang et al. (2001), the temperature dependence of $10^3\ln\alpha_{HCO_3^-(aq)}$-$CO_{2(g)}$ was not considered in their calculations. Carothers' $10^3\ln\alpha_{sid\text{-}CO_{2(g)}}$ values were corrected for this effect in Zhang et al. (2001) and they are plotted in Figure 9a (as "corrected for T"). The corrected values require further adjustment though, because Carothers et al. (1988) also equated the $\delta^{13}C$ values of DIC and $HCO_3^-{}_{(aq)}$, and this assumption is usually invalid below a pH of $\sim$ 7.5 (Romanek et al., 1992). Relating the $\delta^{13}C$ values of DIC and $HCO_3^-{}_{(aq)}$ is somewhat problematic because pH and alkalinity were not reported in Carothers et al. (1988). The correction is likely to be substantial, especially near room temperature, because their solutions were saturated with $CO_{2(g)}$ at a pressure of 4.08 atm. Once this P_{CO_2} was reached, Carothers et al. (1988) heated their hydrothermal vessel to the desired temperature, injected a 1.5 mol/L solution of $FeCl_2$ and raised the total pressure to between 100 to 500 bars by the addition of water to create a single phase solution. The pH of this solution at each temperature (33°, 103°, 150° and 197°C) was calculated using Pitzer's equations and the EQPITZ program (He and Morse, 1993, as amended by Morse, pers. comm.) assuming two phase conditions. Calculated values of pH at 100 to 500 bars ranged from: 1) 6.33 to 6.40 at 33°C, 2) 6.24 to 6.31 at 103°C, 3) 6.19 to 6.25 at 150°C and 4) 6.15 to 6.21 at 197°C. Using average pH values at each temperature, the difference in $\delta^{13}C$ between DIC and $HCO_3^-{}_{(aq)}$ was computed at equilibrium using carbon isotope fractionation factors ($10^3\ln\alpha$) for the $CO_{2(g)}$-$CO_3^{2-}{}_{(aq)}$ (Halas et al., 1997), $HCO_3^-{}_{(aq)}$-$CO_{2(g)}$ (Szaran, 1997), and $CO_{2(g)}$-$CO_{2(aq)}$ (Vogel

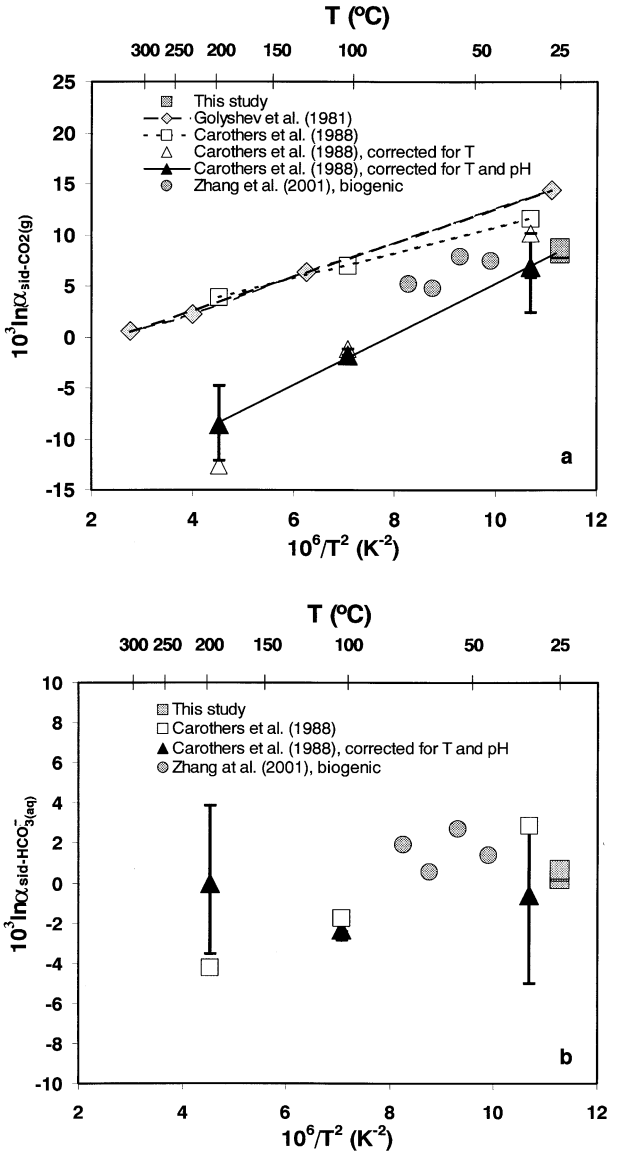

Fig. 9. **a)** Carbon isotope fractionation factor, $10^3\ln\alpha$, for the sid-$CO_{2(g)}$ system for runs CC20, FD-L-3, FD-L-6 and FD-L-9 compared with values published in the literature (Golyshev et al., 1981; Carothers et al., 1988; Zhang et al., 2001). Error bars represent the potential range of $10^3\ln\alpha_{sid\text{-}CO_2(g)}$ values for Carothers et al. (1988) data for pH values ranging from 4 to 8. **b)** Carbon isotope fractionation factors, $10^3\ln\alpha$, for the siderite-$HCO_3^-{}_{(aq)}$ system for the same studies. Symbols and error bars are the same as in Figure 9a.

et al., 1970) systems. The values of $10^3\ln\alpha_{HCO_3^-{}_{(aq)}\text{-}CO_{2(g)}}$ used in this model are identical to those used by Zhang et al. (2001). Halas et al. (1997) determined the carbon isotope fractionation factor for the $CO_3^{=}{}_{(aq)}$-$CO_{2(g)}$ system from 4° to 80°C, and extrapolated their results to 200°C; Szaran (1997) determined carbon isotope fractionation factors for the $HCO_{3(aq)}$-$CO_{2(g)}$ systems from 7° to 70°C, and Vogel et al. (1970) determined the carbon isotope fractionation factor for the $CO_{2(aq)}$-$CO_{2(g)}$ system from 0° to 60°C. Extrapolation of the reported fractionation factors to 150°C and 197°C were required to adjust the $10^3\ln\alpha_{sid\text{-}CO_2(g)}$ values of Carothers et al.

Table 4. Carbon isotope fractionation factors ($10^3\ln\alpha$) for the siderite-CO_2 and siderite-HCO_3^- systems.

sid-$CO_{2(g)}$	T(°C)	$10^3\ln\alpha$	
	0	19.27	
	27	14.33	
	127	6.38	Golishev et al. (1981)
	227	2.20	
	327	0.56	
	33	11.61	
	103	6.98	Carothers et al. (1988)
	150	10.20	
	197	4.53	
	45	7.47	
	55	7.86	Zhang et al. (2001)
	65	4.75	
	75	5.18	
	25	8.5 ± 0.2 (n = 4)	This study

sid-$HCO_{3(aq)}^-$	T(°C)	$10^3\ln\alpha$	
	33	2.86	
	103	−1.74	Carothers et al. (1988)
	150	1.52	
	197	−4.20	
	45	1.37	
	55	2.71	Zhang et al. (2001)
	65	0.55	
	75	1.93	
	25	0.5 ± 0.2 (n = 4)	This study

(1988). The results are tentative at best, but the final corrected $10^3\ln\alpha_{sid\text{-}CO_2(g)}$ value of 8.4 is very close to that obtained in this study (8.5 ± 0.2). The linear trend that fits the corrected data from Carothers et al., (1988) is nearly parallel to that predicted theoretically by Golyshev et al. (1981), although offset to lower values. Carbon isotope fractionation factors ($10^3\ln\alpha_{sid\text{-}CO_2(g)}$) for biogenic siderite by Zhang et al. (2001) are greater than these data but they did not consider the difference in $\delta^{13}C$ between DIC and $HCO_3^-{}_{(aq)}$ at the pH of their experiments.

The average value of $10^3\ln\alpha_{sid\text{-}HCO_3^-{}_{(aq)}}$ from this study was 0.5 ± 0.2, approximately 1.0 higher than that of Carothers et al. (1988) at 33°C, corrected for temperature and DIC-$HCO_{3(aq)}^-$ effects (Fig. 9b), while $10^3\ln\alpha_{sid\text{-}HCO_3^-{}_{(aq)}}$ values determined from biogenic siderite (Zhang et al., 2001) are greater. Considered collectively, $10^3\ln\alpha_{sid\text{-}HCO_3^-{}_{(aq)}}$ values display a relatively wide range and show no clear dependence on temperature, at least for temperatures ranging from 25°C to 197°C.

Values of $10^3\ln\alpha_{sid\text{-}CO_2(g)}$ from this study are close to values reported for other carbonates, although they are lower than isotope fractionation factors for the calcite $CO_{2(g)}$ system determined by Vogel (1961; 9.3 at 22°C), Emrich et al. (1970; 10.2 at 20°C), Turner (1982; 9.0 at 25°C), Romanek et al. (1992; 9.00 ± 0.2 at 25°C), and Jiménez-López et al. (2001; 8.93 ± 0.06 at 25°C). Likewise, $10^3\ln\alpha_{sid\text{-}HCO_3^-{}_{(aq)}}$ values from this study are lower than those from Rubinson and Clayton (1969; 0.9 at 25°C), Romanek et al. (1992; 1.0 ± 0.3 at 25°C) and Jiménez-López et al. (2001; 0.94 ± 0.06 at 25°C).

These results are consistent with the trend that solids are enriched in the isotope of greater mass when they incorporate cations of low mass (i.e., Ca^{2+} versus Fe^{2+}) into the crystal structure (O'Neil, 1986; Bottcher, 2000).

4. CONCLUSIONS

Siderite was precipitated from $NaHCO_3$-$Fe(ClO_4)_2$ solutions under anaerobic conditions at 25°C and 1 atm total pressure using a modified version of the chemo-stat technique and the free-drift technique. The chemo-stat technique permitted somewhat controlled chemical conditions to be maintained during siderite formation. For a given saturation state, siderite precipitation rate was ~ 8 orders of magnitude lower than that of calcite within the range of saturation states investigated. The isotope fractionation factor, $10^3 \ln\alpha$, for the siderite-$CO_{2(g)}$ and siderite-HCO_3^-(aq) systems obtained in these experiments were 8.5 ± 0.2 (1σ; n=4) and 0.5 ± 0.2 (1σ; n=4), respectively, and they agree well with published data for siderite precipitated under different conditions when the effects of temperature and DIC speciation are considered in the calculation of α.

Acknowledgments—This research was partially supported by the Environmental Remediation Sciences Division of the Office of Biologic and Environmental Research, U.S. Department of Energy through the Financial Assistant Award no. DE-FC09-96SR18546 to the University of Georgia Research Foundation, the MEC/Fulbright Program from Spain (FU2000), the NASA Astrobiology Institute (JSC) and NASA's Ancient Martian Meteorite Program. Thanks also go to Dr. Alejandro Rodriguez-Navarro for his help in the SEM analysis, and Lindy Paddock and Brian Jackson for help in the laboratory. We acknowledge Drs S.T. Kim, M. Coleman and one anonymous review for their valuable comments and suggestions.

Associate editor: J. Horita

REFERENCES

Bahrig B. (1985) Paleo-environment information from deep water siderite (Lake of Laach, West Germany). In *Lacustrine Petroleum Source Rocks* (eds. A.J. Fleet, K. Kelts and M.R. Talbot); *Geol. Soc. Spec. Publ.* **40,** 153–158.

Bottcher M. E. (2000) Stable isotope fractionation during experimental formation of Norsethite ($BaMg[CO_3]_2$): A mineral analogue of dolomite. *Aqua. Geochem.* **6,** 201–212.

Bricker O. P. (1985) Environmental factors in the inorganic chemistry of natural systems: the estuarine sediment environment. In *Environmental Inorganic Chemistry* (ed. K. J. Irgolic); Deerfield Beach, Fla. VCH Pub. Chap. 5, 135–153.

Bruno J., Wersin P., and Stumm W. (1992) On the influence of carbonate in mineral dissolution: II. The solubility of $FeCO_3$ (s) at 25°C and 1 atm total pressure. *Geochim. Cosmochim. Acta* **56,** 1149–1155.

Busenberg E. and Plummer L. N. (1986) The solubility of $BaCO_3$(cr) (witherite) in CO_2-H_2O solutions between 0 and 90°C, evaluation of the association constants of $BaHCO_3^{+}{}_{(aq)}$ and $BaCO_3^{0}{}_{(aq)}$ between 5 and 80°C, and a preliminary evaluation of the thermodynamic properties of Ba^{2+}(aq). *Geochim. Cosmochim. Acta* **50,** 2225–2233.

Carothers W. W., Adami L. H., and Rosenbauer R. J. (1988) Experimental oxygen isotope fractionation between siderite-water and phosphoric acid liberated CO_2-siderite. *Geochim. Cosmochim. Acta* **52,** 2445–2450.

Craig H. (1957) Isotopic standards for carbon and oxygen and corrections factor for massspectrometric analysis of carbon dioxide. *Geochim. Cosmochim. Acta* **12,** 133–149.

Coleman M. L. and Raiswell R. (1993) Microbial mineralization of organic matter: Mechanisms of self-organization and inferred rates of precipitation of diagenetic minerals. *Phil. Trans. R. Soc. Lond. A.* **344,** 69–87.

Curtis C. D., Coleman M. L., and Love L. G. (1986) Pore water evolution during sediment burial from isotopic and mineral chemistry of calcite, dolomite and siderite concretions. *Geochim. Cosmochim. Acta* **50,** 2321–2334.

Deleuze M. and Brantley S. (1997) Inhibition of calcite crystal growth by Mg^{2+} at 100°C and 100 bars: Influence of growth regime. *Geochim. Cosmochim. Acta* **7,** 1475–1485.

Dromgoole E. L. and Walter M. (1990a) Iron and manganese incorporation into calcite: Effects of growth kinetics, temperature and solution chemistry. *Chem. Geol.* **81,** 311–336.

Dromgoole E. L. and Walter M. (1990b) Inhibition of calcite growth rates by Mn^{2+} in $CaCl_2$ solutions at 10, 25 and 50°C. *Geochim. Cosmochim. Acta* **54,** 2991–3000.

Duan W. M., Hedrick D. B., Pye K., Coleman M. L., and White D. C. (1996) A preliminary study of the geochemical and microbiological characteristics of modern sedimentary concretions. *Limnol. Oceanogr.* **41,** 1404–1414.

Emerson S. (1976) Early diagenesis in anaerobic lake sediments: Chemical equilibria in interstitial waters. *Geochim. Cosmochim. Acta* **40,** 925–934.

Emrich K., Ehhalt D. H., and Vogel J. C. (1970) Carbon isotope fractionation during the precipitation of calcium carbonate. *Earth Planet. Sci. Lett.* **8,** 363–371.

Faure G. (1991) Principles and applications of inorganic geochemistry. Macmillan Pub. Company, New York, 626 pp.

Fisher Q. J., Raiswell R., and Marshall J. D. (1998) Siderite concretions from nonmarine shales (Westphalian A) of the Pennines England: Controls of their growth and composition. *J. Sediment. Res.* **68,** 1034–1045.

Friedman I, O'Neil J. R (1977) Compilation of stable isotope fractionation factors of geochemical interest. In *Data of Geochemistry* (ed. M. Fleisher) U. S. G. S. Prof. Paper 440-KK, 12 pp.

García-Ruiz J. M. and Amorón J. L. (1980) Sobre la precipitación polimórfica del carbonato cálcico. *Est. Geol.* **36,** 193–200.

Garrels R. M. and Christ C. L. (1990) Solutions, minerals and equilibria. Jones and Bartlett Pub., Boston, 450 pp.

Golyshev S. I., Padalko N. L., and Pechenkin S. A. (1981) Fractionation of stable oxygen and carbon isotopes in carbonate systems. *Geochem. Intl.* **18,** 85–99.

Halas S., Szaran J., and Niezgoda H. (1997) Experimental determination of carbon isotope equilibrium fractionation between dissolved carbonate and carbon dioxide. *Geochim. Cosmochim. Acta* **61 (***13***),** 2691–2695.

Hangari K. M., Ahmad S. N., and Perry E. C. (1980) Carbon and oxygen isotope ratios in diagenic siderite and magnetite from Upper Devonian Ironstone, Wadi Shatti District, Libya. *Econ. Geol.* **75,** 538–545.

He S. and Morse J. W. (1993) The carbonic acid system and calcite solubility in aqueous Na-K-Ca-Mg-Cl-SO_4 solutions from 0 to 90°C. *Geochim. Cosmochim. Acta* **57,** 3533–3554.

Hood G. C., Redlich O., and Reilli C. A. (1954) Ionization of strong electrolytes.3. Proton magnetic resonance in nitric, perchloric, and hydrochloric acids. *J. Chem. Phys.* **22 (***11***),** 2067–2071.

James H. L (1966) Chemistry of the iron-rich sedimentary rocks. *U. S. Geol. Surv. Prof. Paper* 440-W, 61 p.

Jiménez-López C., Caballero E., Huertas F. J., and Romanek C. S. (2001) Chemical, mineralogical and isotopic behavior and phase transformation during the precipitation of calcium carbonate minerals from intermediate ionic solution at 25°C. *Geochim. Cosmochim. Acta* **65 (***19***),** 3219–3231.

Jiménez-López C., Romanek C. S., Huertas F. J., Ohmoto H. and Caballero E. (xxxx) Oxygen isotope fractionation in synthetic magnesian calcite. *Geochim. Cosmochim. Acta* (in press).

Johnson M. L (1990) Ferrous carbonate precipitation kinetics. A temperature ramped approach. Ph. D. Rice University. Houston TX. 1990.

Kazmierczak T. F., Tomsom M. B., and Nancollas G. H. (1982) Crystal growth of calcium carbonate. A controlled composition kinetic study. *J. Phys. Chem.* **86,** 103–107.

Kelts K. (1988) Environments of deposition of lacustrine petroleum source rocks: an introduction. In *Lacustrine Petroleum Source Rocks*

(eds. A. J. Fleet, K. Kelts and M. R. Talbot); *Geol. Soc. Spec. Publ.* **40,** 3–26.

Keller L. P., Thomas K. L., and McKay D. S. (1994) The nature of carbon-bearing phases in hydrated interplanetary dust particles. *Meteoritics* **29 (*4*),** 480–481.

Klein C. and Hurlbut C. S., Jr.. (1985) Manual of mineralogy 20th ed. J. Whiley & Sons Inc., New York, 596 pp.

Lippmann F. (1973) Sedimentary Carbonate Minerals. In *Mineral, Rocks and Inorganic materials* Springer-Verlag Berlin-Heidelberg New York. 228 pp.

Maynard J. B. (1982) Extension of Berner's "New Geochemical Classification of Sedimentary Environments" to ancient sediments. *J. Sediment. Petrol.* **52,** 1325–1331.

McCrea J. (1950) The isotope chemistry of carbonates and a paleotemperature scale. *J. Chem. Phys.* **18,** 849–857.

Meyer H. J. (1984) The influence of impurities on the growth rate of calcite. *J. Cryst. Growth* **66,** 639–646.

Michaelis J., Usdowski E., and Menschel G. (1985) Partitioning of C-13 and C-12 on the degassing of CO_2 and the precipitation of calcite-Rayleigh-type fractionation and a kinetic-model. *Am. J. Sci.* **285,** 318–327.

Michard A., Beucaire C., and Michard G. (1988) Uranium and rare earth elements in CO_2-rich waters from Vals-les-Bains (France). *Geochim. Cosmochim. Acta* **51,** 901–909.

Moore S. E., Ferrell J. R. E., and Aharon P. (1992) Diagenetic siderite and other ferroan carbonates in a modern subsiding marsh sequence. *J. Sediment. Petrol.* **62,** 357–366.

Morse J. W. (1974) Dissolution kinetics of calcium carbonate in sea water. III. A new method for the study of carbonate reaction kinetics. *Am J. Sci.* **274,** 97–107.

Morse J. W. (1978) Dissolution kinetics of calcium carbonate in seawater: IV. The near-equilibrium dissolution kinetics of calcium carbonate-rich deep sea sediments. *Am. J. Sci.* **278,** 344–353.

Morse J. W. and Berner R. A. (1979) The chemistry of calcium carbonate in the deep oceans. In *Chemical Modelling-Speciation, Sorption, Solubility and Kinetics in Aqueous Systems* (ed. E. Jenne), pp. 499–535. Symposium Series 93. American Chemical Society, Washington, DC.

Morse J. W. and Casey W. H. (1988) Ostwald processes and mineral paragenesis in sediments. *Am. J. Sci.* **288,** 537–560.

Mortimer R. J. G. and Coleman M. L. (1997) Microbial influence on the oxygen isotopic composition of diagenetic siderite. *Geochim. Cosmochim. Acta* **61,** 1705–1711.

Mozley P. S. (1989) Relationship between depositional environments and the elemental composition of early diagenetic siderite. *Geology* **17,** 704–706.

Mozley P. S. and Carothers W. W. (1992) Elemental and isotopic composition of siderite in the Kupanuk Formation, Alaska: Effect of microbial activity and water/sediment interaction on early pore-water chemistry. *J. Sediment. Petrol.* **64,** 681–692.

Mucci A. and Morse J. W. (1983) The incorporation of $Mg^{2+}$and Sr^{2+}into calcite overgrowths: Influences of growth rate and solution composition. *Geochim. Cosmochim. Acta* **47,** 217–233.

Mucci A. (1987) Influence of temperature on the composition of magnesian calcite overgrowth precipitated from seawater. *Geochim. Cosmochim. Acta* **51,** 1977–1984.

Nancollas G. H. and Reddy M. M. (1971) The crystallization of calcium carbonate II. Calcite growth mechanism. *J. Colloid Int. Sci.* **37,** 824–830.

Nordstrom D. K., Plummer L. N., Langmuir D., Busenberg E., May H. M., Jones B. F. and Parkhurst D. L. (1990) Revised chemical equilibrium data for mayor water-mineral reactions and their limitations. In *Chemical Modeling of Aqueous Systems II, ACS Symposium Series* **416,** 390–413.

Ogino T., Suzuki T., and Sawada K. (1987) The formation and transformation mechanism of calcium carbonate in water. *Geochim. Cosmochim. Acta* **51,** 2757–2767.

O'Neil J. R. (1986) Theoretical and experimental aspects of isotope fractionation. In Stable isotopes in high temperature geological process. *Rev. Mineral.* **16,** 1–41.

Perry E. C., Jr. and Tan F. C. (1972) Significance of oxygen and carbon isotope variations in early Precambrian cherts and carbonate rocks of southern Africa. *Geol. Soc. America Bull.* **83,** 647–664.

Ptacek C. J (1992) Experimental determination of siderite solubility in high ionic-strength aqueous solutions. Ph. D. Thesis, Univ. Waterloo, Waterloo, Ontario, Canada.

Rajan S., Mackenzie F. T., and Glenn C. R. (1996) A thermodynamic model for water column precipitation of siderite in the Plio-Pleistocene Black Sea. *Am. J. Sci.* **296,** 506–548.

Reddy M. M. and Nancollas G. H. (1971) The crystallization of Calcium Carbonate. I. Isotope exchange and kinetics. *J. Coll. Int. Sci.* **36,** 166–172.

Reddy M. M. and Wang K. K. (1980) Crystallization of calcium carbonate in the presence of metal ions. I. Inhibition by magnesium ion at pH 8.8 and 25°C. *J. Cryst. Growth.* **50,** 470–480.

Romanek C. S., Grossman E. L., and Morse J. W. (1992) Carbon isotopic fractionation in synthetic calcite, effects of temperature and precipitation rate. *Geochim. Cosmochim. Acta* **56,** 419–430.

Romanek C. S., Grady M. M., Wright I. P., Mittlefehldt D. W., Socki R. A., Pillinger C. T., and Gibson E. K., Jr... (1994) Record of fluid-rock interactions on Mars from the meteorite ALH84001. *Nature* **372,** 655–430.

Romanek C. S., Zhang C. L., Li Y., Vali H., Horita J., and Cole D. R. (2003) Carbon and hydrogen isotope fractionations asscoaited with dissimilatory iron-reducing bacteria. *Chem. Geol.(Isot. Geosci. Sect.)* **195,** 5–16.

Rubinson M. and Clayton R. N. (1969) Carbon-13 fractionation between aragonite and calcite. *Geochim. Cosmochim. Acta* **33,** 997–1002.

Sears G. W. (1961) The origin of spherulites. *J. Chem. Phys.* **65,** 1738–1741.

Singer P. C. and Stumm W. (1970) The solubility of ferrous iron in carbonate-bearing waters. *J. Am. Water Works Assoc.* **62,** 198–202.

Stumm W. and Morgan J. J. (1981) Aquatic Chemistry. Wiley Interscience, New York, pp. 780.

Szaran J. (1997) Achievement of carbon isotope equilibrium in the system HCO_3^- (solution) -CO_2(gas). *Chem. Geol.* **142,** 79–86.

Thyne G. D. and Gwinn C. J. (1994) Evidence for a paleoaquifer from early diagenetic siderite of the cardium formation, Alberta, Canada. *J. Sed. Res.* **A64 (*4*),** 726–732.

Treiman A. H. and Romanek C. S. (1998) Bulk and stable isotopic composition of carbonate minerals in Martian meteorite Allan Hills 84001: No proof of high formation temperature. *Meteor. Planet. Sci.* **33,** 737–742.

Turner J. V. (1982) Kinetic fractionation of carbon-13 during calcium carbonate precipitation. *Geochim. Cosmochim. Acta* **46,** 1183–1191.

Usdowski E., Hoefs J., and Menschel G. (1979) Relationship between C-13 and O-18 fractionation and changes in major element composition in a recent calcite-depositing spring. Model of chemical variations with inorganic $CaCO_3$ precipitation. *Earth Planet. Sci. Lett.* **42 (*2*),** 267–276.

Usdowski E. and Hoefs J. (1990) Kinetic $^{13}C/^{12}C$ and $^{18}O/^{16}O$ effects upon dissolution and outgassing of CO_2 in the system CO_2-H_2O. *Chem. Geol. (Isot. Geosci. Sect.)* **80,** 109–118.

Valley J. W., Eiler J. M., Graham C. M., Gibson E. K., Jr., Romanek C. S., and Stolper E. M. (1997) Low-temperature carbonate concretions in the Martian meteorites ALH 84001: Evidence from stable isotopes and mineralogy. *Science* **275,** 1633–1638.

Vogel J. C. (1961) Isotope separation factors of carbon in the equilibrium system CO_2-$HCO_3^-$$CO_3^{2-}$. *Proc. Summer Course Nucl. Geol., Varenna (1960).* 216–221.

Vogel J. C., Grootes P. M., and Mook W. G. (1970) Isotopic fractionation between gaseous and dissolved carbon dioxide. *Z. Phys.* **230,** 225–238.

Wersin P., Charlet L., Karthein R., and Stumm W. (1989) From adsorption to precipitation: Sorption of Mn^{2+} on $FeCO_3$(s). *Geochim. Cosmochim. Acta* **53,** 2787–2796.

Zhang C. L., Vali H., Romanek C. S., Roh Y., Sears S. K., and Phelps T. J. (1998) Chemical and morphological characterization of siderite formed by iron reducing bacteria. *Am. Mineral.* **61,** 927–932.

Zhang C. L., Horita J., Cole D. R., Zhou J., Lovley D. R., and Phelps T. J. (2001) Temperature-dependent oxygen and carbon isotope fractionation of biogenic siderite. *Geochim. Cosmochim. Acta* **65 (*14*),** 2257–2271.